Gastroenterology 2020;159:682–709

SETDB1 Inhibits p53-Mediated Apoptosis and Is Required for Formation of Pancreatic Ductal Adenocarcinomas in Mice

Satoshi Ogawa,[1] Akihisa Fukuda,[1] Yoshihide Matsumoto,[1] Yuta Hanyu,[1] Makoto Sono,[1] Yuichi Fukunaga,[1,2] Tomonori Masuda,[1] Osamu Araki,[1] Munemasa Nagao,[1] Takaaki Yoshikawa,[1] Norihiro Goto,[1] Yukiko Hiramatsu,[1] Motoyuki Tsuda,[1] Takahisa Maruno,[1] Yuki Nakanishi,[1] Mohammed S. Hussein,[1,3] Tatsuaki Tsuruyama,[4] Kyoichi Takaori,[5] Shinji Uemoto,[5] and Hiroshi Seno[1]

[1]Department of Gastroenterology and Hepatology, Kyoto University Graduate School of Medicine, Kyoto, Japan; [2]Department of Drug Discovery Medicine, Medical Innovation Center, Kyoto University Graduate School of Medicine, Kyoto, Japan; [3]Department of Internal Medicine, Al-Azhar University, Cairo, Egypt; [4]Clinical Bioresource Center, Kyoto University Hospital, Kyoto, Japan; and [5]Division of Hepato-Biliary-Pancreatic Surgery and Transplantation, Department of Surgery, Kyoto University Graduate School of Medicine, Kyoto, Japan

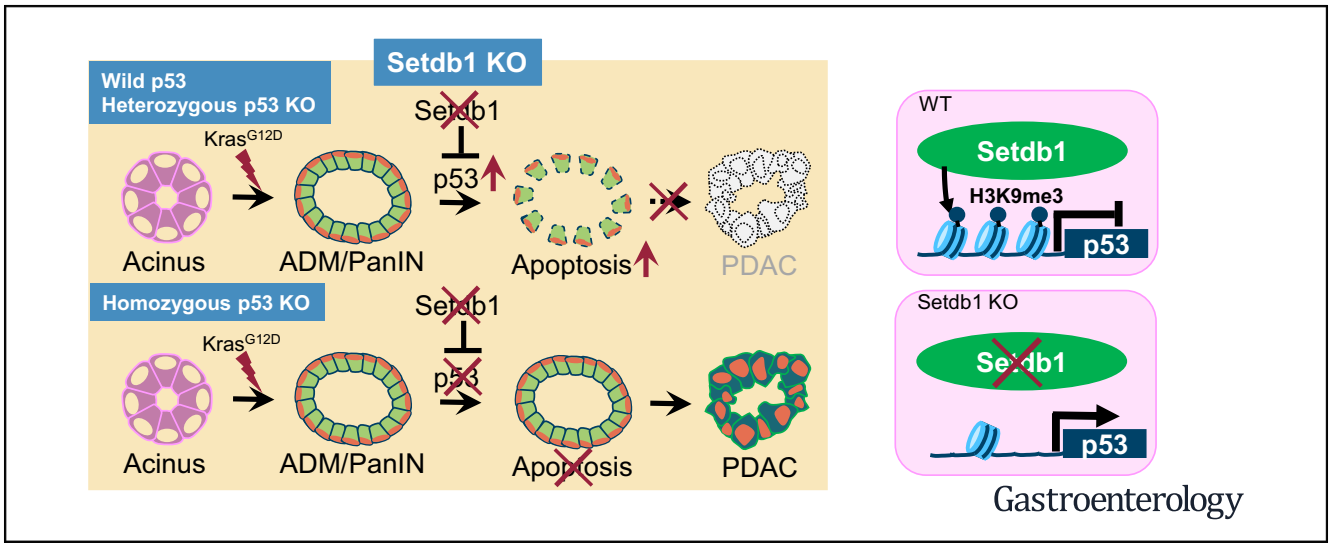

See editorial on page 437.

BACKGROUND & AIMS: SETDB1, a histone methyltransferase that trimethylates histone H3 on lysine 9, promotes development of several tumor types. We investigated whether SETDB1 contributes to development of pancreatic ductal adenocarcinoma (PDAC). **METHODS:** We performed studies with *Ptf1a*^{Cre}; *Kras*^{G12D}; *Setdb1*$^{f/f}$, *Ptf1a*^{Cre}; *Kras*^{G12D}; *Trp53*$^{f/+}$; *Setdb1*$^{f/f}$, and *Ptf1a*^{Cre}; *Kras*^{G12D}; *Trp53*$^{f/f}$; *Setdb1*$^{f/f}$ mice to investigate the effects of disruption of *Setdb1* in mice with activated KRAS-induced pancreatic tumorigenesis, with heterozygous or homozygous disruption of *Trp53*. We performed microarray analyses of whole-pancreas tissues from *Ptf1a*^{Cre}; *Kras*^{G12D}; *Setdb1*$^{f/f}$, and *Ptf1a*^{Cre}; *Kras*^{G12D} mice and compared their gene expression patterns. Chromatin immunoprecipitation assays were performed using acinar cells isolated from pancreata with and without disruption of *Setdb1*. We used human PDAC cells for SETDB1 knockdown and inhibitor experiments. **RESULTS:** Loss of SETDB1 from pancreas accelerated formation of premalignant lesions in mice with pancreata that express activated KRAS. Microarray analysis revealed up-regulated expression of genes in the apoptotic pathway and genes regulated by p53 in SETDB1-deficient pancreata. Deletion of *Setdb1* from pancreas prevented formation of PDACs, concomitant with increased apoptosis and up-regulated expression of *Trp53* in mice heterozygous for disruption of *Trp53*. In contrast, pancreata of mice with homozygous disruption of *Trp53* had no increased apoptosis, and PDACs developed. Chromatin immunoprecipitation revealed that SETDB1 bound to the *Trp53* promoter to regulate its expression. Expression of an inactivated form of SETDB1 in human PDAC cells with wild-type *TP53* resulted in TP53-induced apoptosis. **CONCLUSIONS:** We found that the histone methyltransferase SETDB1 is required for development of PDACs, induced by activated KRAS, in mice. SETDB1 inhibits apoptosis by regulating expression of p53. SETDB1 might be a therapeutic target for PDACs that retain p53 function.

Keywords: Pancreatic Cancer; Oncogene; Cell Death; Epigenetic Factor.

Pancreatic ductal adenocarcinoma (PDAC) is one of the most dismal malignancies, with an extremely poor prognosis.[1] In order to further improve the prognosis, it is crucial to elucidate the molecular mechanisms underlying PDAC initiation and progression.

Recent studies have revealed that epigenetic abnormalities exhibit a great influence on the characteristics of cancer development in addition to genetic abnormalities.[2–4] One form of epigenetic regulation, known as histone modification, contributes to tumorigenesis by affecting the expression of oncogenes/tumor suppressor genes. In fact, previous reports have shown that histone methyltransferases suppress pancreatic cancer by regulating glucose/fatty acid metabolism and promoting pancreatic regeneration.[5,6]

Setdb1 serves as a histone 3 lysine 9 trimethyltransferase. Trimethylation of histone 3 lysine 9 (H3K9me3) is a repressive chromatin modification.[7] Setdb1 plays different functional roles through gene silencing. It helps to control heterochromatin formation[8] and contributes to stem cell maintenance,[9] embryonic development, and endogenous proviral silencing.[10] Recently, an in vivo study revealed that the amplification of *Setdb1* accelerates the development of melanoma,[11] and SETDB1 has been shown to promote tumorigenesis in various human cancers, including lung,[12] liver,[13,14] and breast cancers.[15] Furthermore, a whole-exome sequencing study revealed a copy number amplification mutation of *SETDB1* in PDAC patients.[16] These findings indicate a role of Setdb1 in PDAC initiation and progression. However, the functional role of Setdb1 in PDAC remains elusive. Therefore, in this study, we aimed to investigate the impact of *Setdb1* deletion on Kras-induced pancreatic tumorigenesis and elucidate the in vivo role of Setdb1 in PDAC formation in mouse models.

WHAT YOU NEED TO KNOW

BACKGROUND AND CONTEXT

SETDB1, a histone methyltransferase that trimethylates histone H3 on lysine 9, promotes development of several tumor types, but it is not clear if it contributes to development of pancreatic ductal adenocarcinoma (PDAC).

NEW FINDINGS

SETDB1 is required for development of PDACs, induced by activated KRAS, in mice. SETDB1 inhibits apoptosis by regulating expression of p53.

LIMITATIONS

Future studies are required to clarify the role of SETDB1 in p53 mutated PDAC.

IMPACT

SETDB1 might be a therapeutic target for PDACs that retain p53 function.

Materials and Methods

Mice

Experimental animals were generated by crossing *Ptf1a*^{Cre} (gift from Y. Kawaguchi, Kyoto University, Kyoto, Japan),[17] *Kras*^{G12D} (gift from D. Tuveson, Cold Spring Harbor Laboratory, Cold Spring Harbor, NY),[18] *Setdb1*^{flox} (gift from Y. Shinkai, Riken, Saitama, Japan),[10] and *p53*^{flox} (purchase from Jackson Laboratory, Bar Harbor, ME; JAX strain 008462).

Acute pancreatitis was induced at 6 weeks of age by injecting cerulein (2 μg/injection diluted in phosphate-buffered saline; Sigma-Aldrich, St Louis, MO) intraperitoneally on 2 consecutive days once every hour for 8 hours each day.[19]

Clinical Samples

Forty-eight surgically resected specimens of pancreatic cancer tissues were obtained from patients who had been admitted to Kyoto University Hospital. Written informed consent was obtained from all patients and the protocol was approved by the Ethics Committee of Kyoto University.

Cell Lines

A mouse acinar cell line (266-6) was purchased from ATCC (Manassas, VA), and cultured on 0.1% gelatin-coated plate in Dulbecco's modified Eagle medium supplemented with 10% fetal bovine serum. Human PDAC cell lines (PK59 and KP4) were purchased from RIKEN (Tsukuba, Japan), and cultured in RPMI medium supplemented with 10% fetal bovine serum. For inhibition experiments, cells were cultured in growth medium containing 10% fetal bovine serum overnight at 37°C under 5% CO_2 on a 6-well plate. Then, the plates were treated with mithramycin at defined concentrations or dimethyl sulfoxide for 3 days. Total RNA was extracted from PDAC cell lines administered with mithramycin for 3 days using RNA mini Kit.

Statistics

Data are presented as mean ± SEM. Statistical comparisons between groups were made using the Student *t* test or Cochran-Armitage test. *P* values <.05 were considered as statistically significant. All statistical analyses were performed with either GraphPad Prism, version 6.0 (GraphPad, La Jolla, CA), JMP 15 (SAS Institute Inc, Cary, NC), or Microsoft Excel 2016 (Microsoft, Redmond, WA).

Study Approval

All mice experiments were approved by the animal research committee of Kyoto University and performed in accordance with Japanese government regulations. Surgically resected specimens of pancreatic cancer tissues were obtained from patients who had been admitted to Kyoto University Hospital. Written informed consent was obtained from all patients and

Abbreviations used in this paper: **ADM, acinar-to-ductal metaplasia; ChIP, chromatin immunoprecipitation; CK19, cytokeratin 19; H3K9me3, histone H3 on lysine 9 tri-methylation; *KC*, *Ptf1a*^{Cre}; *Kras*^{G12D}; *KCS*, *Ptf1a*^{Cre}; *Kras*^{G12D}; *Setdb1*$^{f/f}$; KO, *Ptf1a*^{Cre}; *Setdb1*$^{f/f}$; *KP*^{hetero}*C*, *Ptf1a*^{Cre}; *Kras*^{G12D}; *p53*$^{f/+}$; PanIN, pancreatic intraepithelial neoplasia; PDAC, pancreatic ductal adenocarcinoma; qRT-PCR, quantitative reverse transcription polymerase chain reaction.**

Most current article

0016-5085
https://doi.org/10.1053/j.gastro.2020.04.047

the protocol was approved by the Ethics Committee of Kyoto University.

Detailed methods are described in the Supplementary Material and Methods. Primary antibodies are listed in Supplementary Table 1. Primer Sequences are described in Supplementary Table 2.

Results

Setdb1 was Dispensable for Pancreatic Development

To determine the expression pattern of Setdb1 in pancreatic epithelial cells in mice, we first performed immunohistochemistry. Setdb1 was expressed in pancreatic ductal cells and a small subset of acinar cells in wild-type mice (Figure 1*A* and *B*). During cerulein-induced pancreatitis, Setdb1 was expressed in ductal cells, almost all acinar cells, and acinar-to-ductal metaplasia (ADM) (Figure 1*A* and *B*). In *Ptf1a*^{Cre}; *Kras*^{G12D} (*KC*) or *Ptf1a*^{Cre}; *Kras*^{G12D}; *p53*$^{f/+}$ (*KP*^{hetero}*C*) mice, a well-established mouse model of PDAC, Setdb1 was expressed in ADM, pancreatic intraepithelial neoplasia (PanIN), and PDAC (Figure 1*A* and *B*). Also, Western blot analysis revealed that Setdb1 and H3K9me3 were expressed in PanIN and PDAC tissues from *KC* and *KP*^{hetero}*C* mice, respectively (Figure 1*C*). In addition, enzyme activity of H3K9 methyltransferase was observed in mouse PanIN and PDAC tissues, respectively (Figure 1*D*). Consistent with the expression pattern in mice, in humans, SETDB1 was expressed in pancreatic ductal cells and a subset of acinar cells in normal pancreas (Figure 1*E*). Further immunohistochemical analysis revealed positive SETDB1 expression in 21 out of 48 PDAC cases (Figure 1*E* and *F*).

To investigate the possible functional requirement of Setdb1 for pancreatic development and maintenance, we generated *Ptf1a*^{Cre}; *Setdb1*$^{f/f}$ mice. *Ptf1a*^{Cre}; *Setdb1*$^{f/f}$ mice were born as predicted by the Mendelian ratio and were indistinguishable from control *Ptf1a*^{Cre} mice. *Ptf1a*^{Cre}; *Setdb1*$^{f/f}$ mice were indistinguishable from control mice in terms of pancreata appearance and the pancreas/body weight ratio at 6 weeks of age. Histologically, *Ptf1a*^{Cre}; *Setdb1*$^{f/f}$ mice showed no pancreatic abnormalities at that time point (Supplementary Figure 1*A*). Efficient recombination of the *Setdb1* allele was confirmed in *Ptf1a*^{Cre}; *Setdb1*$^{f/f}$ pancreata by quantitative reverse transcription polymerase chain reaction (qRT-PCR) (Supplementary Figure 1*B*). These data suggested that Setdb1 was dispensable for pancreatic development in mice.

Setdb1 Was Required for Exocrine Pancreatic Regeneration

Given that Setdb1 was expressed in ADM, we next determined whether Setdb1 plays a role in exocrine pancreas regeneration in response to cerulein-induced acute pancreatitis, which induced ADM. Two and 7 days after cerulein treatment, in contrast to control *Ptf1a*^{Cre} mice, massive pancreatic atrophy and severe reduction in the pancreas to body weight ratio were observed in *Ptf1a*^{Cre}; *Setdb1*$^{f/f}$ mice (Figure 2*A* and *B*). Histologically, 2 days after cerulein treatment, infiltration of inflammatory cells and ADM formation were induced due to acute pancreatitis in control *Ptf1a*^{Cre} mice. In contrast, more massive infiltration of inflammatory cells was observed concomitant with increased ductal structures and fewer acinar cells in *Ptf1a*^{Cre}; *Setdb1*$^{f/f}$ mice compared with control mice (Figure 2*C*, Supplementary Figure 2*A*). In addition, the pathology score of pancreatitis was significantly higher in *Ptf1a*^{Cre}; *Setdb1*$^{f/f}$ mice compared to control mice (Figure 2*D*). These findings suggested that Setdb1 loss resulted in the exacerbations of pancreatitis in the early acute phase. Seven days after cerulein treatment, prolonged pancreatitis was observed in *Ptf1a*^{Cre}; *Setdb1*$^{f/f}$ mice, whereas pancreatitis was almost fully recovered in control mice (Figure 2*C* and *D*).

To better characterize the immune cell populations infiltrating in *Ptf1a*^{Cre}; *Setdb1*$^{f/f}$ pancreata 2 days and 7 days after cerulein treatments, we performed immunostaining for F4/80, CD45, CD3, CD8, CD11b, and CD117. The immunostaining and quantification results revealed that the number of F4/80-, CD45-, CD3-, or CD11b-positive cells was significantly increased in *Ptf1a*^{Cre}; *Setdb1*$^{f/f}$ mice compared to the controls 2 days and 7 days after treatment (Figure 2*C* and *D*, Supplementary Figure 2*A* and *B*). The infiltration of F4/80-positive cells was remarkably observed in *Ptf1a*^{Cre}; *Setdb1*$^{f/f}$ mice. The infiltration of CD8- or CD117-positive cells was rarely observed in both control and *Ptf1a*^{Cre}; *Setdb1*$^{f/f}$ mice. These data indicated that pancreatic deletion of *Setdb1* exacerbated the cerulein-induced pancreatitis and that pancreatic Setdb1 was required for normal exocrine pancreas regeneration after cerulein-induced pancreatitis.

To investigate the underlying mechanisms for the pancreas atrophy in *Ptf1a*^{Cre}; *Setdb1*$^{f/f}$ mice upon pancreatitis, we evaluated cell proliferation and apoptosis in *Ptf1a*^{Cre} and *Ptf1a*^{Cre}; *Setdb1*$^{f/f}$ mice 2 days after cerulein treatment. Immunostaining for cleaved caspase 3 and terminal deoxynucleotidyl transferase–mediated deoxyuridine triphosphate nick-end labeling (TUNEL) staining revealed a dramatic increase in apoptotic cells in *Ptf1a*^{Cre}; *Setdb1*$^{f/f}$ mice compared to control *Ptf1a*^{Cre} mice, whereas immunostaining for Ki67 revealed that there were no differences in cell proliferation between the control and *Ptf1a*^{Cre}; *Setdb1*$^{f/f}$ mice (Figure 3*A*–*C*). To investigate the possible mechanism of *Setdb1* deletion-mediated apoptosis upon pancreatitis, we performed immunostaining for p53, which is one of the major players for apoptosis, and found that p53 expression was markedly increased in *Ptf1a*^{Cre}; *Setdb1*$^{f/f}$ mice 2 days after cerulein treatment (Figure 3*D* and *E*). Consistently, qRT-PCR analysis revealed that the expression of apoptotic genes, including *Apaf1*, *Noxa*, and *p53*, was significantly elevated in *Ptf1a*^{Cre}; *Setdb1*$^{f/f}$ mice compared to control mice, whereas the expression of an anti-apoptotic gene, *Bcl2*, was significantly decreased (Figure 3*F* and *G*). In a physiological condition, *p53* expression was comparable between *Ptf1a*^{Cre} and *Ptf1a*^{Cre}; *Setdb1*$^{f/f}$ mice (Supplementary

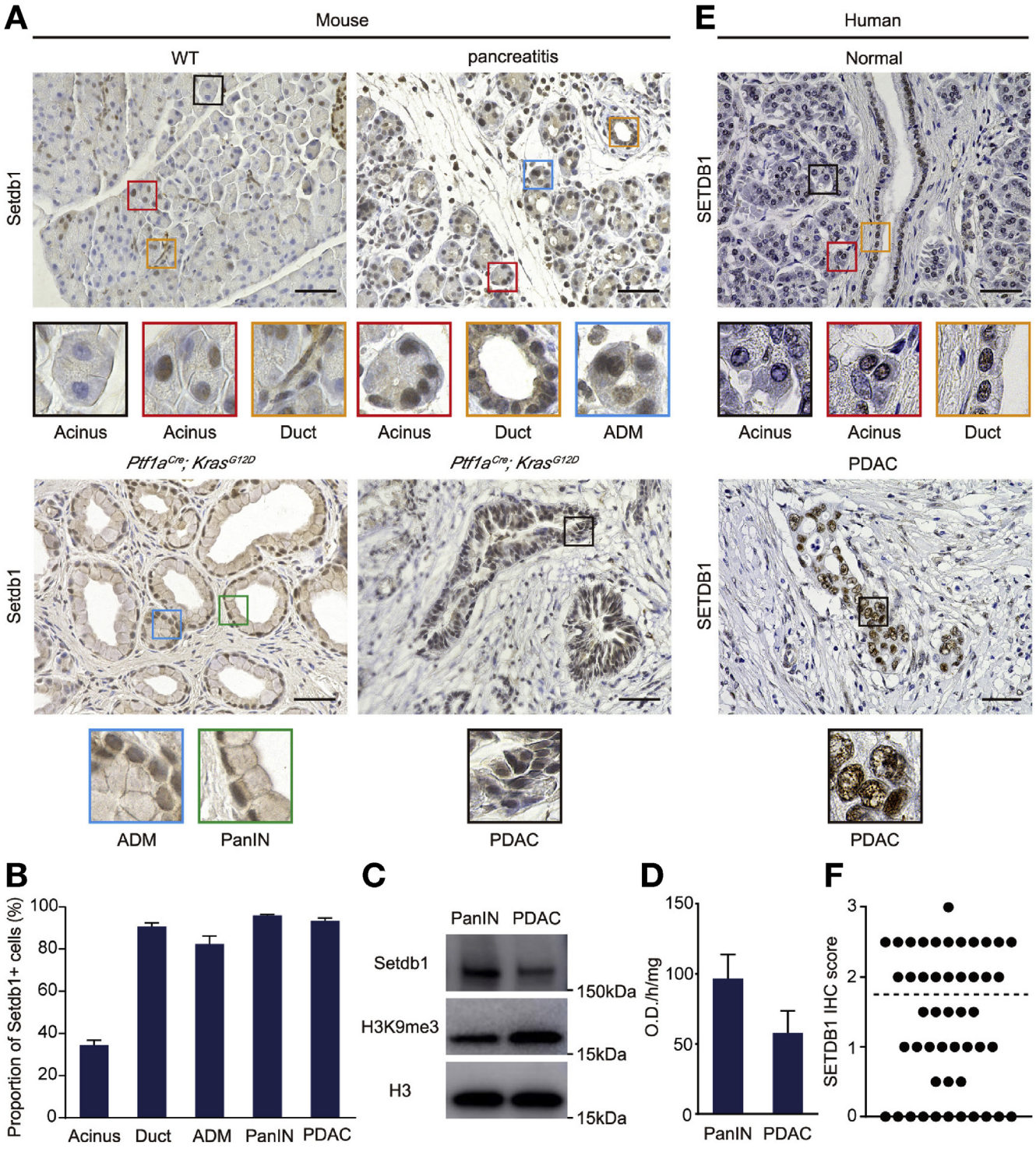

Figure 1. The expression of Setdb1 in mouse and human pancreas. (*A*) Representative immunostaining for Setdb1 in wild-type (WT) mice (*upper left*) at 6 weeks of age, cerulein-induced pancreatitis (*upper right*) 2 days after cerulein treatment at 6 weeks of age, and *Ptf1a*^{Cre}*; Kras*^{G12D} (*KC*) mice at 20 and 48 weeks of age or *Ptf1a*^{Cre}*; Kras*^{G12D}*; p53*$^{f/+}$ (*KP*^{hetero}*C*) mice at 20 weeks of age (*lower 2*) ($n = 3$). Scale bars: 50 μm. (*B*) Proportion of Setdb1-positive cells in all acinar cells in WT, duct cells in WT mice, ADM in pancreatitis, PanIN in *KC* mice, and PDAC cells in *KC* or *KP*^{hetero}*C* mice, respectively, in random high-power fields (n = 3). Means ± SEM are shown. (*C*) Western blot analysis for Setdb1 and H3K9me3 using PanIN and PDAC tissues from *KC* and *KP*^{hetero}*C* mice, respectively (n = 3). (*D*) Quantification of H3K9 methyltransferase activity in PanIN and PDAC tissues from *KC* and *KP*^{hetero}*C* mice, respectively (n = 3). Means ± SEM are shown. (*E*) Representative immunostaining for SETDB1 in human normal pancreas (*upper*) and PDAC (*lower*) tissues. Scale bars: 50 μm. (*F*) SETDB1 immunohistochemistry (IHC) score ranging from 0 to 3 (0 = none, 1 = low, 2 = medium, 3 = high) evaluated by 2 investigators from 48 human PDAC samples. The cutoff score was <2 for negative and ≥ 2 for positive SETDB1 expression.

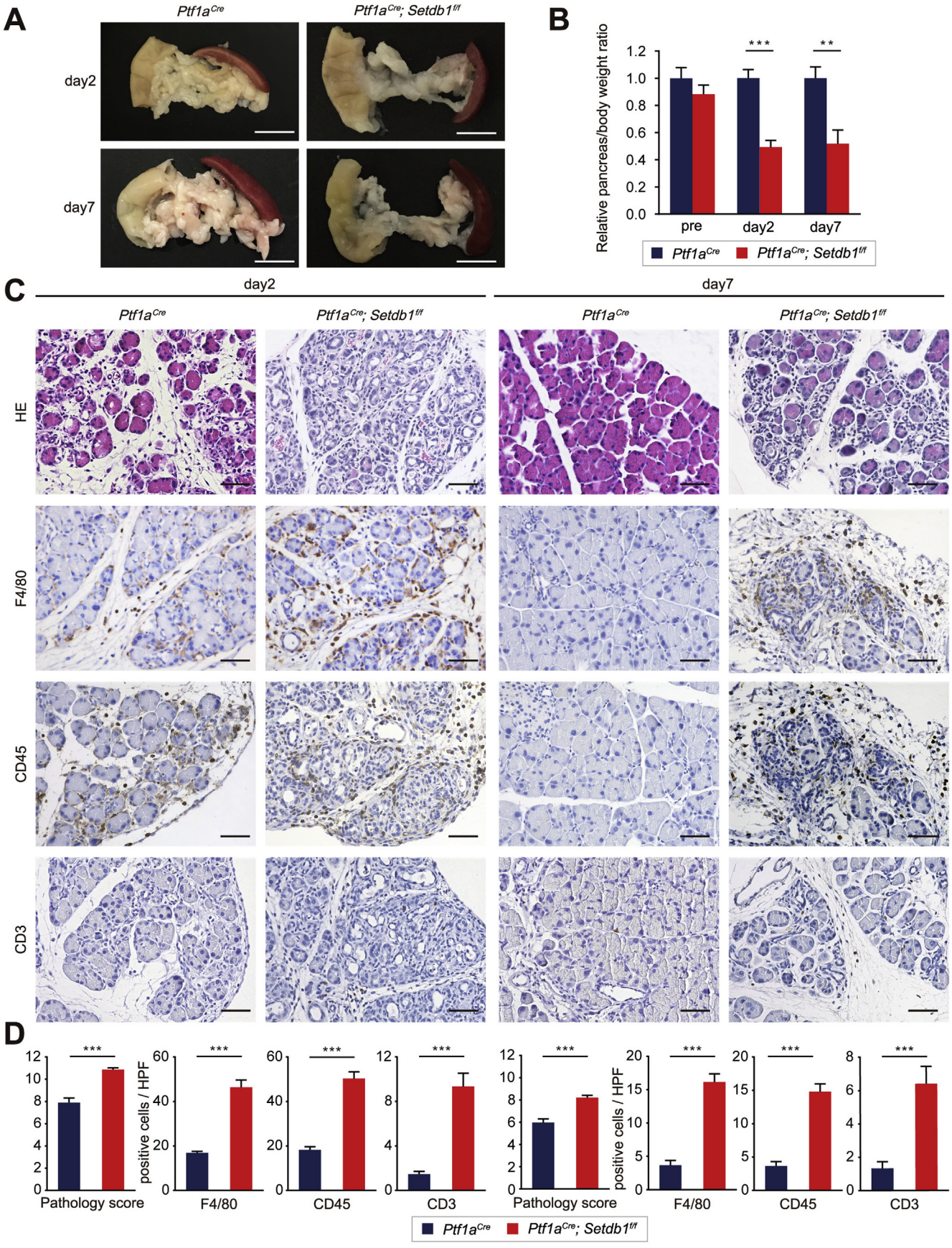
A
Ptf1a^Cre
Ptf1a^Cre; Setdb1^f/f
day2
day7
B
Relative pancreas/body weight ratio
1.2
1.0
0.8
0.6
0.4
0.2
0.0
***
**
pre
day2
day7
Ptf1a^Cre
Ptf1a^Cre; Setdb1^f/f
C
day2
day7
Ptf1a^Cre
Ptf1a^Cre; Setdb1^f/f
Ptf1a^Cre
Ptf1a^Cre; Setdb1^f/f
HE
F4/80
CD45
CD3
D
***
positive cells / HPF
Pathology score
F4/80
CD45
CD3
Pathology score
positive cells / HPF
F4/80
CD45
CD3
Ptf1a^Cre
Ptf1a^Cre; Setdb1^f/f

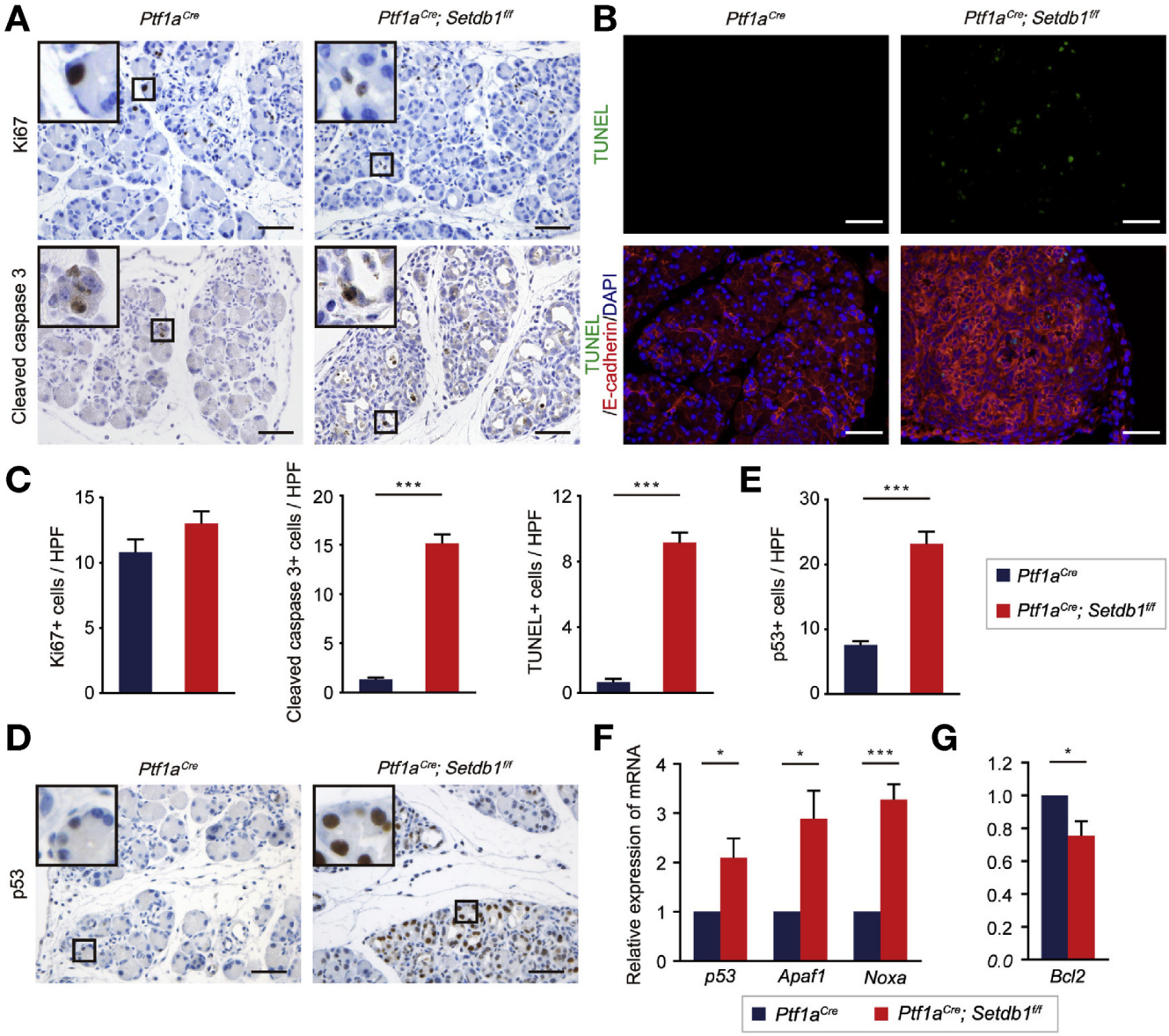

Figure 3. *Setdb1* deletion induced apoptosis and up-regulated p53 expression after cerulein-induced pancreatitis. (*A*) Representative immunostaining for Ki67 (*upper row*) and cleaved caspase 3 (*lower row*) in *Ptf1a*^{Cre} and *Ptf1a*^{Cre}*; Setdb1*$^{f/f}$ mice 2 days after cerulein treatment (n = 3). Scale bars: 50 μm. (*B*) Representative terminal deoxynucleotidyl transferase–mediated deoxyuridine triphosphate nick-end labeling (TUNEL) staining (*green, upper row*), and co-immunostaining of E-cadherin (*red*) and TUNEL staining (*lower row*), counterstaining with 4′,6-diamidino-2-phenylindole (DAPI) (*blue*) in *Ptf1a*^{Cre} and *Ptf1a*^{Cre}*; Setdb1*$^{f/f}$ mice 2 days after cerulein treatment (n = 3). Scale bars: 50 μm. (*C*) Numbers of Ki67-, cleaved caspase 3–, and TUNEL-positive cells/high-power field (HPF) (n = 3). Means ± SEM are shown. (*D*) Representative immunostaining for p53 in *Ptf1a*^{Cre} and *Ptf1a*^{Cre}*; Setdb1*$^{f/f}$ mice 2 days after cerulein treatment (n = 3). Scale bars: 50 μm. (*E*) Numbers of p53-positive cells/HPF (n = 3). Means ± SEM are shown. (*F, G*) qRT-PCR analysis of apoptotic genes (*F*) and an anti-apoptotic gene (*G*) in *Ptf1a*^{Cre} and *Ptf1a*^{Cre}*; Setdb1*$^{f/f}$ mice 2 days after cerulein treatment (n = 5). Means ± SEM are shown. **P* < .05; ***P* < .01; ****P* < .001, Student *t* test.

Figure 2. Pancreatic *Setdb1* deletion led to pancreatic atrophy and exacerbated cerulein-induced pancreatitis. (*A*) Representative gross morphology of *Ptf1a*^{Cre} and *Ptf1a*^{Cre}*; Setdb1*$^{f/f}$ pancreata at 6 weeks of age 2 days after cerulein treatment (*top row*) and 7 days after cerulein treatment (*bottom row*) (n = 5–7). Scale bars: 5 mm. (*B*) Relative pancreas to body weight ratio in mice at 6 weeks of age before or after cerulein treatment (n = 5–7). Means ± SEM are shown. (*C*) Representative H&E staining and immunostaining for F4/80, CD45, and CD3 in *Ptf1a*^{Cre} and *Ptf1a*^{Cre}*; Setdb1*$^{f/f}$ mice 2 days after cerulein treatment (*left 2 rows*) (n = 3) and 7 days after cerulein treatment (*right 2 rows*) (n = 3). Scale bars: 50 μm. (*D*) Pathology score of pancreatitis and numbers of F4/80-, CD45-, and CD3-positive cells/HPFs in *Ptf1a*^{Cre} and *Ptf1a*^{Cre}*; Setdb1*$^{f/f}$ mice 2 days (*left 4 graphs*) and 7 days (*right 4 graphs*) after treatment with cerulein (n = 3). Means ± SEM are shown. **P* < .05; ***P* < .01; ****P* < .001, Student *t* test.

Figure 3). These results indicated that pancreatic deletion of *Setdb1* resulted in pancreatic atrophy concomitant with increased apoptosis and up-regulated p53 expression after cerulein-induced pancreatitis.

Setdb1 *Deletion Accelerated the Formation of Acinar-to-Ductal Metaplasia/Pancreatic Intraepithelial Neoplasia in the Context of Oncogenic Kras Activation*

The expression of Setdb1 in ADM, PanIN, and PDAC implied the possible role of Setdb1 in pancreatic tumorigenesis. Furthermore, given that pancreatic deletion of *Setdb1* exacerbated the cerulein-induced pancreatitis, we next investigated the impact of pancreatic *Setdb1* deletion in the context of oncogenic Kras activation. To this end, we generated $Ptf1a^{Cre}$; $Kras^{G12D}$; $Setdb1^{f/f}$ (*KCS*) mice and compared them to control $Ptf1a^{Cre}$; $Kras^{G12D}$ (*KC*) mice. Histologically, at 1 week of age, *KCS* pancreata were indistinguishable from *KC* pancreata, as indicated by H&E staining. However, at 4 and 8 weeks of age, duct-like structures and fibrosis could be observed in *KCS* pancreata more prominently compared to *KC* pancreata, suggesting that Setdb1 loss resulted in the exacerbations of metaplastic ductal change with fibrosis in the context of oncogenic Kras (Supplementary Figure 4*A*). To characterize the duct-like structures observed in *KCS* pancreata at 4 and 8 weeks of age, we first performed immunostaining for amylase, cytokeratin 19 (CK19), sex determining region Y box 9 (Sox9), phosphorylated extracellular signal–regulated kinase (pErk), and phosphorylated signal transducer and activator of transcription 3 (pStat3) (Supplementary Figure 4*B*). Notably, immunostaining displayed amylase- and CK19 double-positive cells indicative of ADM in *KCS* pancreata at 4 weeks of age, whereas these were not observed in *KC* controls. To quantify the PanIN and fibrotic areas, we performed immunostaining for Claudin 18 and Sirius Red staining, respectively. Quantification analysis revealed that areas of PanIN and fibrosis were markedly increased in *KCS* mice compared to *KC* mice (Supplementary Figure 4*C*–*E*). These data indicated that pancreatic deletion of *Setdb1* markedly accelerated the formation of ADM/PanIN with fibrosis in the context of oncogenic Kras activation.

To investigate whether the phenotypes observed in pancreatic *Setdb1* deleted mice was cell autonomous or non–cell autonomous, we next isolated acinar cells from $Ptf1a^{Cre}$; $Setdb1^{f/f}$ mice at 6 weeks of age, cultured them in a 3-dimensional culture system, and compared to those from control $Ptf1a^{Cre}$ mice. In the absence of transforming growth factor–α, significantly higher number of acinar cells from $Ptf1a^{Cre}$; $Setdb1^{f/f}$ mice converted to duct-like cysts compared to those from control $Ptf1a^{Cre}$ mice. When treated with transforming growth factor–α, the formation rate of ductal cystic structures in $Ptf1a^{Cre}$; $Setdb1^{f/f}$ mice was significantly higher than that in control $Ptf1a^{Cre}$ mice (Supplementary Figure 5*A* and *B*). Immunostaining for amylase and CK19 revealed that this ductal cystic structure was ADM (Supplementary Figure 5*C*), supporting our in vivo data that ADM formation was more prominent in $Ptf1a^{Cre}$; $Setdb1^{f/f}$ mice. These data suggested that acinar cells from $Ptf1a^{Cre}$; $Setdb1^{f/f}$ mice had the characteristics to convert to ductal cells, at least in part, in a cell autonomous manner ex vivo.

To understand the underlying mechanism whereby Setdb1 loss predisposed acinar cells to retain ductal phenotype in $Ptf1a^{Cre}$; $Setdb1^{f/f}$ mice, we performed qRT-PCR of acinar cells isolated from $Ptf1a^{Cre}$ and $Ptf1a^{Cre}$; $Setdb1^{f/f}$ mice at 6 weeks of age, and qRT-PCR of *KC* and *KCS* pancreata at 1 week of age. However, there was no significant difference between expressions of pancreatic transcription factors of both groups (Supplementary Figure 6*A* and *B*). We also evaluated the activation of mediators related to Wnt pathway, Notch pathway, and inflammation in *KC and KCS* pancreata at 1 week of age by qRT-PCR analysis. However, there were no significant differences among them between *KC* and *KCS* pancreata (Supplementary Figure 6*C*–*E*). These data suggested that pancreatic transcription factors, Wnt pathway, Notch pathway, and inflammation were not mainly involved in enhanced ADM/PanIN formation in *KCS* pancreata.

Setdb1 *Deletion Led to Increased Apoptosis and Elevated p53 Expression*

Given the fact that apoptosis was increased during cerulein-induced pancreatitis, we next evaluated apoptotic status in *KCS* pancreata at 4 weeks of age. Immunostaining for cleaved caspase 3 and TUNEL staining revealed a significant increase in the numbers of apoptotic cells in *KCS* pancreata compared to *KC* pancreata (Figure 4*A*–*C*).

To identify the global transcriptional changes in *KCS* pancreata, we performed genome-wide analysis of gene expression in *KC* and *KCS* pancreata at 4 weeks of age. Microarray analysis of messenger RNA from *KC* and *KCS* pancreata demonstrated that the expression of genes related to apoptotic pathways were up-regulated (Figure 4*D*). Pathway enrichment analyses (gene ontology analysis) using the software program DAVID 6.8 (https://david.ncifcrf.gov/) showed that the apoptotic process (GO: 0006915) was significantly enriched (false discovery rate, 9.9E-11). Furthermore, the genes related to apoptotic processes, such as *Tns4*, *p19*, *Serpina3g*, *Noxa*, *Trfrs11b*, and *S100a8*, were included among the 100 most up-regulated genes in *KCS* mice compared to *KC* mice (Supplementary Figure 7). Notably, Gene Set Enrichment Analysis revealed that "apoptotic signaling pathway" and "p53 downstream pathway" were significantly enriched in *KCS* pancreata compared to *KC* pancreata (Figure 4*E*). Furthermore, the qRT-PCR analysis confirmed that the expression of apoptotic genes, including *p53, Apaf1*, and *Noxa*, was elevated, whereas the expression of an anti-apoptotic gene *Bcl2* was decreased, in *KCS* pancreata compared to *KC* pancreata (Figure 4*F* and *G*). These results indicated that pancreatic *Setdb1* deletion led to up-regulation of the apoptotic signaling pathway and p53 pathway in the context of oncogenic Kras activation.

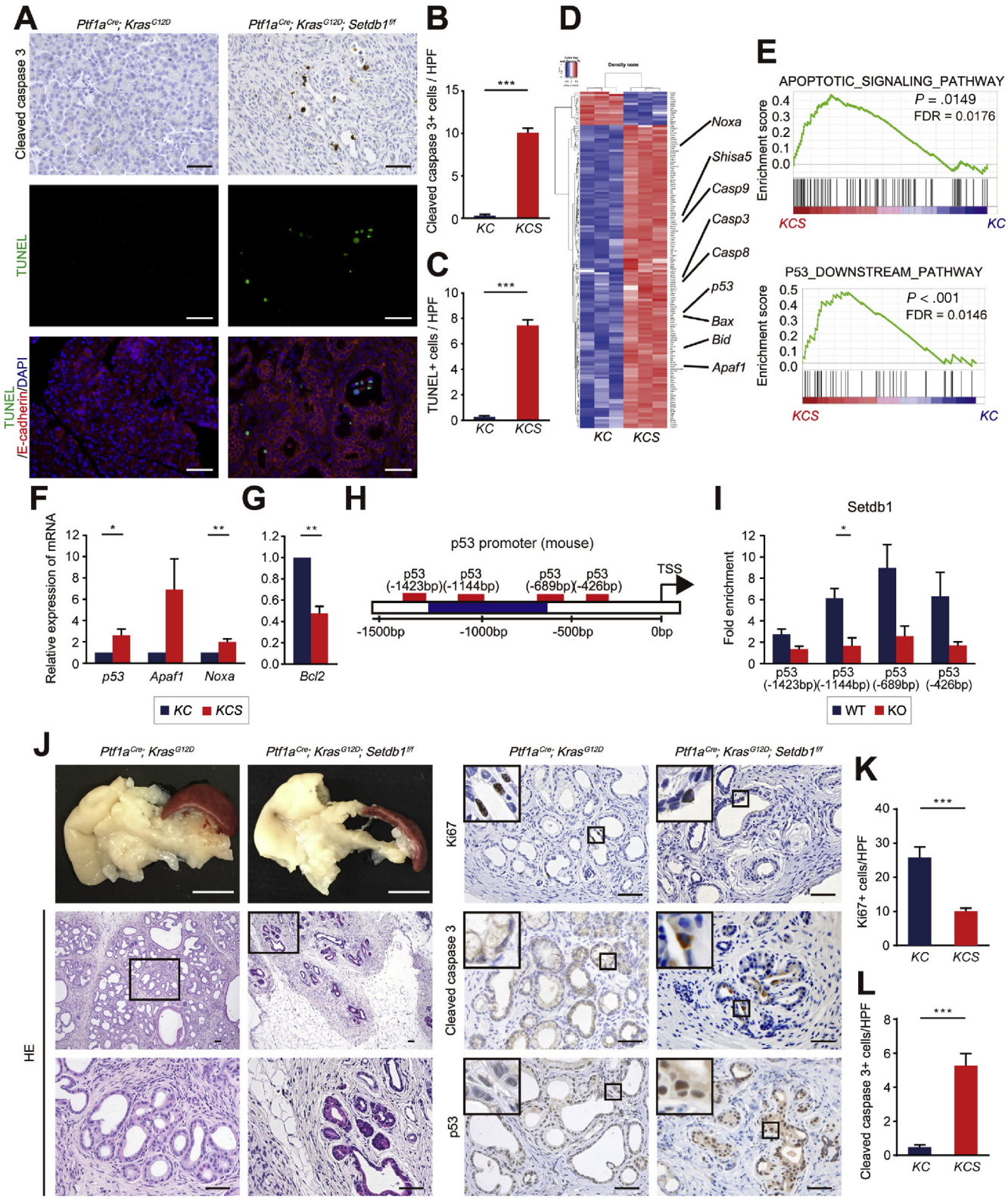
A
Ptf1a^Cre; Kras^G12D
Ptf1a^Cre; Kras^G12D; Setdb1^f/f
Cleaved caspase 3
TUNEL
TUNEL /E-cadherin/DAPI
B
Cleaved caspase 3+ cells / HPF
***
KC
KCS
C
TUNEL+ cells / HPF
***
KC
KCS
D
Density none
Noxa
Shisa5
Casp9
Casp3
Casp8
p53
Bax
Bid
Apaf1
KC
KCS
E
APOPTOTIC_SIGNALING_PATHWAY
P = .0149
FDR = 0.0176
Enrichment score
KCS
KC
P53_DOWNSTREAM_PATHWAY
P < .001
FDR = 0.0146
Enrichment score
KCS
KC
F
Relative expression of mRNA
p53
Apaf1
Noxa
KC
KCS
G
Bcl2
H
p53 promoter (mouse)
p53 (-1423bp)
p53 (-1144bp)
p53 (-689bp)
p53 (-426bp)
TSS
-1500bp
-1000bp
-500bp
0bp
I
Setdb1
Fold enrichment
p53 (-1423bp)
p53 (-1144bp)
p53 (-689bp)
p53 (-426bp)
WT
KO
J
Ptf1a^Cre; Kras^G12D
Ptf1a^Cre; Kras^G12D; Setdb1^f/f
HE
Ki67
Cleaved caspase 3
p53
K
Ki67+ cells/HPF
***
KC
KCS
L
Cleaved caspase 3+ cells/HPF
***
KC
KCS

Setdb1 Bound to p53 *Promoter Regions to Directly Regulate its Expression*

Given that p53 expression was increased in *KCS* mice and that Setdb1 has been determined as an essential factor for apoptosis associated with p53,[12,20] we next investigated whether Setdb1 directly regulates p53 expression in the pancreas. To address this question, we performed chromatin immunoprecipitation (ChIP) assay using acinar cells isolated from wild-type and $Ptf1a^{Cre}$; $Setdb1^{f/f}$ (KO) mice at 6 weeks of age. The ChIP-sequencing data of a previous report showed that Setdb1 binding was enriched in *p53* promoter regions of mouse embryonic stem cells.[21] Therefore, we designed primers around this area and performed ChIP experiments (Figure 4*H*). ChIP experiments revealed that Setdb1 bound to the promoter regions of *p53* in isolated acinar cells of wild-type mice. In contrast, we found that Setdb1 binding was impaired in isolated acinar cells of KO mice (Figure 4*I*). These results suggested that Setdb1 bound to *p53* promoter regions to directly regulate its expression in the pancreas.

Setdb1 *Deletion Promoted Pancreatic Atrophy With Increased Apoptosis in the Context of Oncogenic Kras*

At 20 weeks of age, higher degree of pancreatic atrophy was observed in *KCS* mice compared to *KC* mice (Figure 4*J*). Histologically, almost all acinar cells were replaced by ADM and PanIN in *KC* mice. In contrast, pancreatic parenchyma was replaced by fibrosis and fat in *KCS* mice, as indicated by H&E staining (Figure 4*J*). Immunostaining for Ki67 revealed significant cell proliferation in *KC* mice, whereas it was not observed in *KCS* mice. Of note, immunostaining for cleaved caspase 3 and p53 showed dramatic increase in apoptotic cells and p53 expression in *KCS* mice compared to *KC* mice (Figure 4*J*). Quantification analysis revealed that the number of cleaved caspase 3–positive cells was significantly increased in *KCS* mice compared to *KC* mice, whereas the number of Ki67 positive cells was significantly decreased in *KCS* mice compared to *KC* mice (Figure 4*K* and *L*). These data indicated that *Setdb1* deletion led to increased apoptosis, and subsequently, pancreatic atrophy in the context of oncogenic Kras.

Setdb1 *Deletion Protected Against Pancreatic Ductal Adenocarcinoma Formation in the Context of Heterozygous* p53 *Deletion*

Given that *Setdb1* deletion led to increased apoptosis in the context of oncogenic Kras, we next investigated the impact of pancreatic *Setdb1* deletion on PDAC formation. To this end, we crossed *KCS* mice with $p53^{f/+}$ mice to generate $Ptf1a^{Cre}$; $Kras^{G12D}$; $p53^{f/+}$; $Setdb1^{f/f}$ ($KP^{hetero}CS$) mice and compared them to control $Ptf1a^{Cre}$; $Kras^{G12D}$; $p53^{f/+}$; $Setdb1^{wt/wt}$ ($KP^{hetero}C$) mice at 20 weeks of age. Gross morphology showed that $KP^{hetero}CS$ pancreata were more atrophic compared to $KP^{hetero}C$ pancreata. Histologically, control $KP^{hetero}C$ mice displayed PDAC formation at 20 weeks of age, whereas no PDAC formation was observed in $KP^{hetero}CS$ mice at that age, as indicated by H&E staining (Figure 5*A*). Immunostaining for Ki67 revealed that prominent cell proliferation was observed in PDAC in control $KP^{hetero}C$ mice, whereas it was not observed in $KP^{hetero}CS$ mice. Of note, immunostaining for cleaved caspase 3 and p53 showed markedly increased apoptotic cells and up-regulated p53 expression in $KP^{hetero}CS$ mice compared to that in control $KP^{hetero}C$ mice. Quantification analysis revealed that the number of cleaved caspase 3–positive cells was significantly increased, whereas the number of Ki67-positive cells was markedly decreased in $KP^{hetero}CS$ mice compared to control mice (Figure 5*A*–*C*). We found that all control $KP^{hetero}C$ mice developed PDAC (6 of 12 mice succumbed to PDAC before censor, and the other 6 mice developed PDAC at 20–24 weeks of age). Surprisingly, none of 5 $KP^{hetero}CS$ mice developed PDAC at 24 weeks of age (Figure 5*D*). Kaplan-Meier curves analysis revealed that

Figure 4. *Setdb1* deletion caused p53-mediated apoptosis and massive pancreatic atrophy. Moreover, Setdb1 bound to the *p53* promoter regions. (*A*) Representative immunostaining for cleaved caspase 3 (*top row*) and terminal deoxynucleotidyl transferase–mediated deoxyuridine triphosphate nick-end labeling (TUNEL) staining (*green, middle row*), and co-immunostaining of E-cadherin (*red*) and TUNEL staining (*bottom row*), counterstaining with 4′,6-diamidino-2-phenylindole (DAPI) (*blue*) in *KC* and *KCS* at 4 weeks of age (n = 3). Scale bars: 50 μm. (*B, C*) Numbers of cleaved caspase 3– (*B*) and TUNEL- (*C*) positive cells/high-power field (HPF) in *KC* and *KCS* at 4 weeks of age (n = 3). Means ± SEM are shown. (*D*) A heatmap showing the expression of genes related to apoptotic process, comparing *KC* and *KCS* pancreata at 4 weeks of age (n = 3). (*E*) Enrichment plots from gene set enrichment analysis (GSEA) shows that apoptotic signaling pathway was up-regulated in *KCS* pancreata. The GO_APOPTOTIC_SIGNALING_PATHWAY gene set contains a series of molecular signals, which triggers the apoptotic death of a cell (*upper*). The PID_P53_DOWNSTREAM_PATHWAY gene set contains direct p53 effectors (*lower*). Nominal *P* value and false discovery rate *q* value are shown in each GSEA plot. (*F, G*) qRT-PCR analysis of apoptotic genes (*F*) and an anti-apoptotic gene (*G*) in *KC* and *KCS* at 4 weeks of age (n = 5). Means ± SEM are shown. (*H*) Illustration of the murine *p53* promoter sites. *Black arrow* indicates the transcription start site. *Red bar* shows the sites investigated by ChIP assay. *Blue bar* shows the enrichment area in Setdb1 ChIP sequencing data of mouse embryonic stem cells (GSM440256).[21] (*I*) ChIP-qPCR of isolated acinar cells from wild-type (WT) and $Ptf1a^{Cre}$; $Setdb1^{f/f}$ (KO) mice at 6 weeks of age in the promoter regions of *p53* (n = 2–4). Means ± SEM are shown. Relative fold enrichment of Setdb1 over IgG control. *Numbers* in primer names show distance from transcription start site. (*J*) *Left 2 rows*: Representative gross morphology of *KC* and *KCS* pancreata at 20 weeks of age (*top row*) (n = 3). Scale bars: 5 mm. H&E staining in KC and KCS mice at 20 weeks of age (*lower 2 rows*) (n = 3). *Right 2 rows*: Representative immunostaining for Ki67, cleaved caspase 3, and p53 in *KC* and *KCS* mice at 20 weeks of age (n = 3). Scale bars: 50 μm. (*K, L*) Numbers of Ki67- (*K*) and cleaved caspase 3– (*L*) positive cells/HPF in *KC* and *KCS* mice at 20 weeks of age (*n* = 3). Means ± SEM are shown. **P* < .05; ***P* < .01; ****P* < .001, Student *t* test.

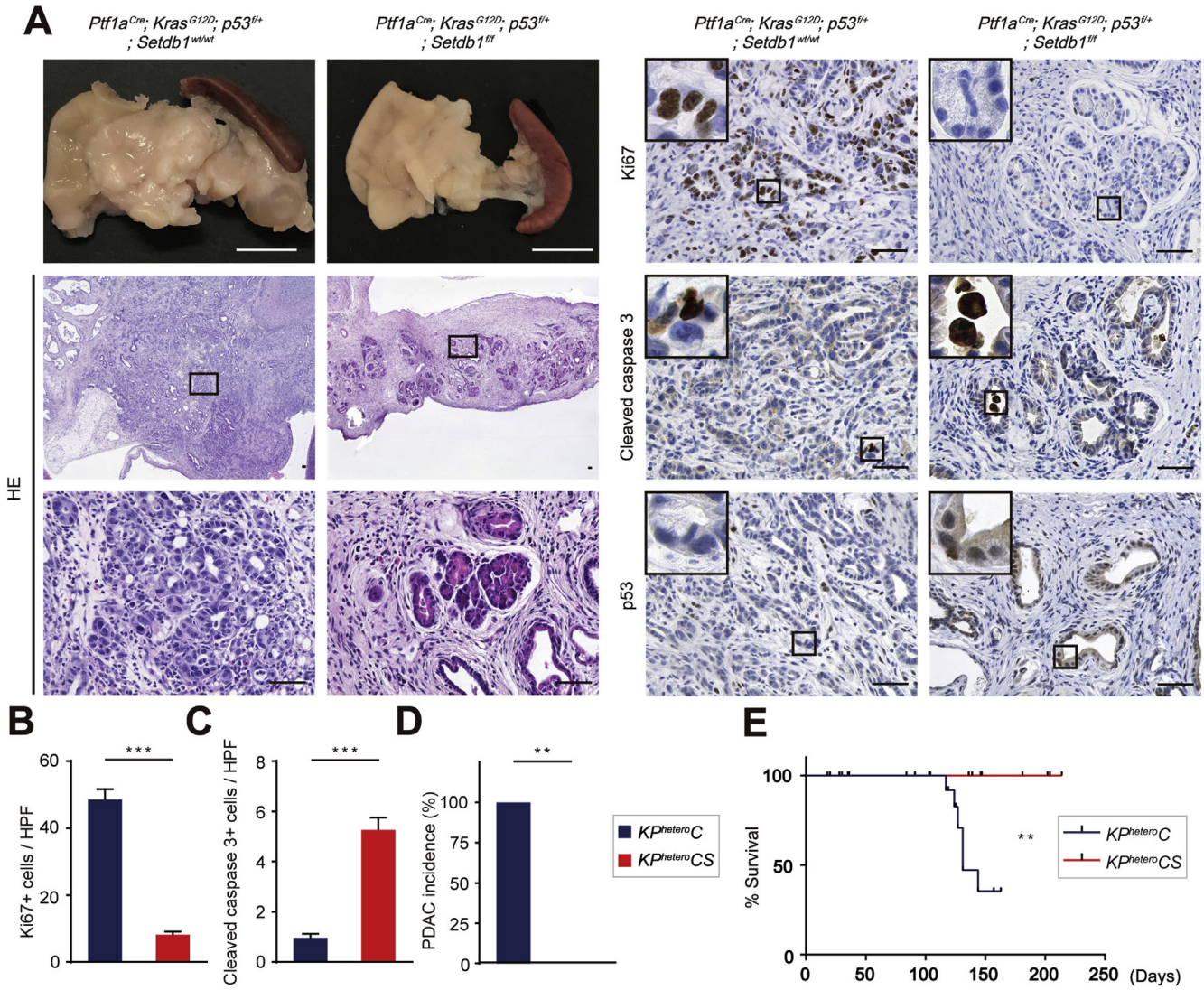

Figure 5. *Setdb1* deletion prevented PDAC formation with increased apoptosis in the context of heterozygous *p53* deletion. (*A*) *Left 2 rows:* Representative gross morphology of $KP^{hetero}C$ and $KP^{hetero}CS$ pancreata at 20 weeks of age (*top row*). Scale bars: 5 mm. Representative H&E staining in $KP^{hetero}C$ and $KP^{hetero}CS$ mice at 20 weeks of age (*lower row*) (n = 4–6). *Right 2 rows*: Representative immunostaining for Ki67, cleaved caspase 3, and p53 in $KP^{hetero}C$ and $KP^{hetero}CS$ mice at 20 weeks of age (n = 3). Scale bars: 50 μm. (*B, C*) Numbers of Ki67- (*B*) and cleaved caspase 3– (*C*) positive cells/high-power field (HPF) in $KP^{hetero}C$ and $KP^{hetero}CS$ mice at 20 weeks of age (n = 3). Means ± SEM are shown. (*D*) PDAC incidence in $KP^{hetero}C$ (n = 6) and $KP^{hetero}CS$ (n = 5) mice at 24 weeks of age. (*E*) Kaplan-Meier survival curve of $KP^{hetero}C$ (n = 17) and $KP^{hetero}CS$ (n = 17) mice. *$P < .05$; **$P < .01$; ***$P < .001$, Student *t* test and log-rank test.

$KP^{hetero}CS$ mice showed significantly better prognosis for survival compared to control $KP^{hetero}C$ mice (Figure 5*E*). These findings indicated that *Setdb1* deletion prevented from PDAC formation while inducing apoptosis and up-regulating p53 expression in the context of heterozygous *p53* deletion.

Suppression of Pancreatic Ductal Adenocarcinoma Formation by Setdb1 *Deletion Was Offset in the Absence of p53*

Given that Setdb1 directly regulated p53 expression in the pancreas and that *Setdb1* deletion protected against PDAC formation while inducing apoptosis and up-regulating p53 expression in the context of heterozygous *p53* deletion, we next determined whether suppression of PDAC formation by *Setdb1* deletion is offset by homozygous p53 deletion. To this end, we generated $Ptf1a^{Cre}$; $Kras^{G12D}$; $p53^{f/f}$; $Setdb1^{f/f}$ ($KP^{homo}CS$) mice and compared them to control $Ptf1a^{Cre}$; $Kras^{G12D}$; $p53^{f/f}$; $Setdb1^{wt/wt}$ ($KP^{homo}C$) mice at 6 weeks of age. Gross morphology and H&E staining showed PDAC formation in both control $KP^{homo}C$ and $KP^{homo}CS$ mice (Figure 6*A*). Immunostaining for Ki67, CK19, pErk, and pStat3 revealed that there were no apparent differences between PDAC of control $KP^{homo}C$ and $KP^{homo}CS$ mice (Figure 6*A*). In addition, immunostaining for cleaved caspase 3 and p53 showed that there

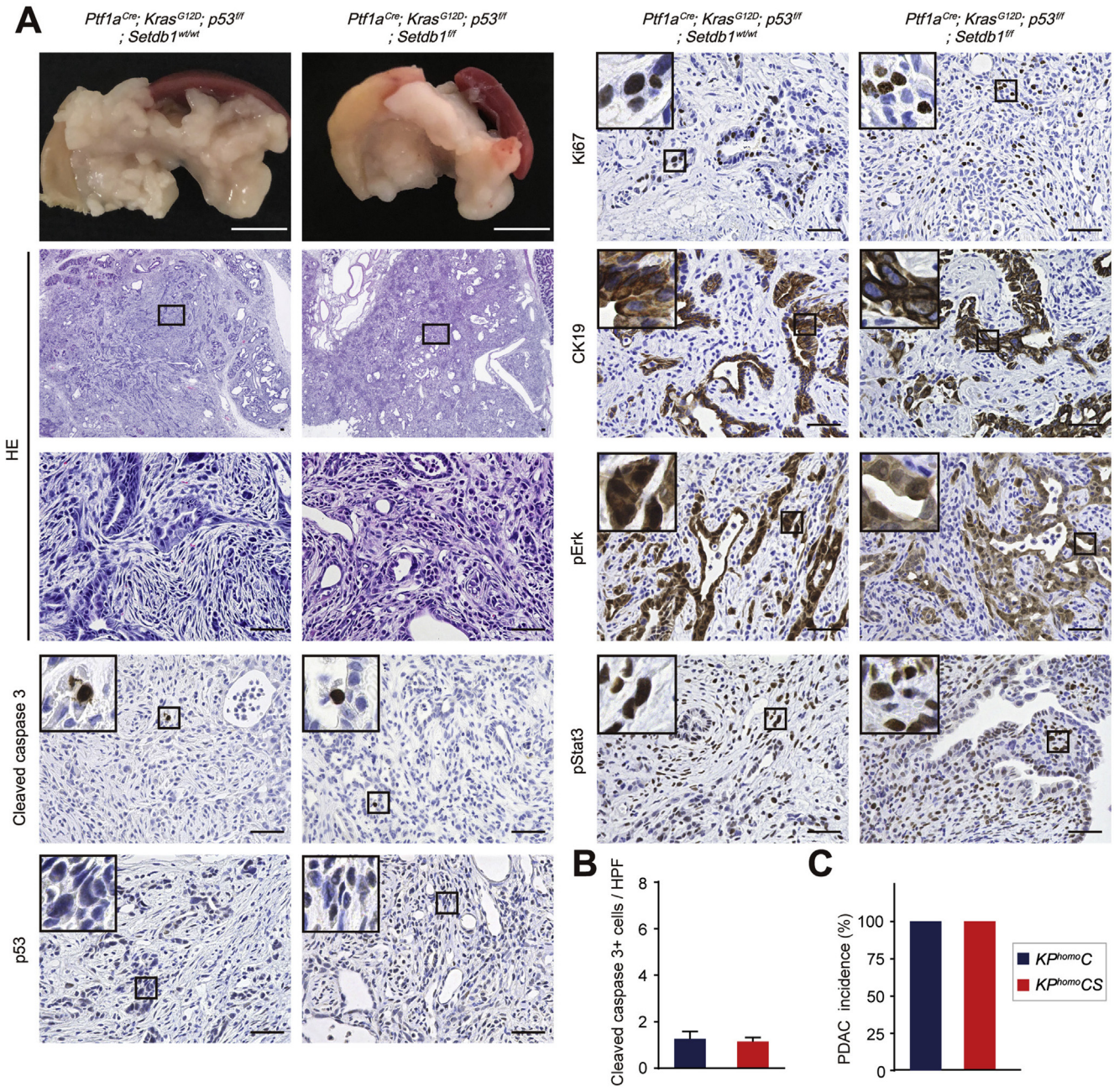

Figure 6. Homozygous *p53* deletion offset protection against PDAC formation and increased apoptosis by *Setdb1* deletion. (*A*) *Left 2 rows:* Representative gross morphology of $KP^{homo}C$ and $KP^{homo}CS$ pancreata at 6 weeks of age (*top row*). Scale bars: 5 mm. Representative H&E staining and immunostaining for cleaved caspase 3 and p53 in $KP^{homo}C$ and $KP^{homo}CS$ mice at 6 weeks of age (n = 3). Scale bars: 50 μm. *Right 2 rows*: Representative immunostaining for Ki67, CK19, phosphorylated extracellular signal-regulated kinase (pErk), and phosphorylated signal transducer and activator of transcription 3 (pStat3) in $KP^{homo}C$ and $KP^{homo}CS$ mice at 6 weeks of age (n = 3). Scale bars: 50 μm. (*B*) Numbers of cleaved caspase 3–positive cells/high-power field (HPF) in $KP^{homo}C$ and $KP^{homo}CS$ at 6 weeks of age (n = 3). Means ± SEM are shown. (*C*) PDAC incidence in $KP^{homo}C$ (*n* = 5) and $KP^{homo}CS$ (n = 7) mice at 6 weeks of age. $^{*}P < .05$; $^{**}P < .01$; $^{***}P < .001$, Student *t* test.

were no apparent differences between control $KP^{homo}C$ and $KP^{homo}CS$ mice (Figure 6*A*). Quantification showed that there was no significant difference in the number of cleaved caspase 3–positive cells between control $KP^{homo}C$ and $KP^{homo}CS$ mice (Figure 6*B*). Notably, we found that all control $KP^{homo}C$ mice (5 of 5 mice) and all $KP^{homo}CS$ mice (7 of 7 mice) developed PDAC at 6 weeks of age (Figure 6*C*). These results indicated that homozygous *p53*

deletion offset increased apoptosis and suppression of PDAC formation by *Setdb1* deletion in $KP^{homo}CS$ mice.

Taken together, these results indicated that pancreatic *Setdb1* deletion protected against PDAC formation by inducing p53-meditaed apoptosis.

Given that the status of the RAS-MYC oncogenic axis is important for the regenerative program, which is involved in PDAC initiation,[22,23] we investigated whether the RAS-MYC oncogenic axis is altered in *KCS* mice. We found that the expression of *c-Myc* expression was significantly decreased in *KCS* mice compared to control mice (Supplementary Figure 8). Given that Myc co-operates with Ras to play various roles in PDAC formation, the down-regulated Ras-Myc oncogenic axis may

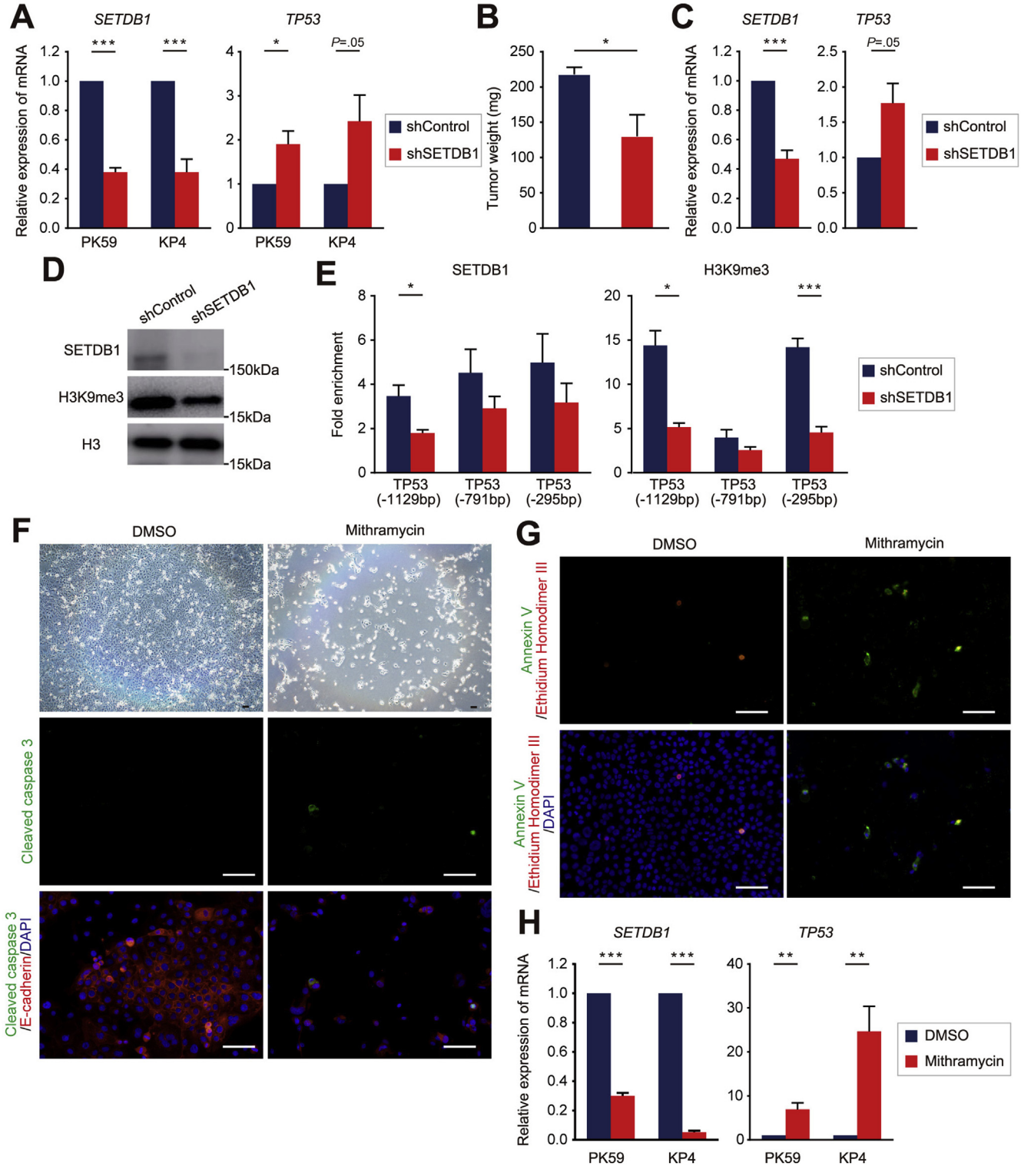

also play a tumor-suppressive role in PDAC formation in *KCS* mice.

Suppression of SETDB1 Led to Elevated TP53 Expression and Reduced Growth of Human Pancreatic Ductal Adenocarcinoma Cells

We next investigated whether suppression of SETDB1 affects TP53 expression and growth of human PDAC cells. To this end, we silenced SETDB1 and performed growth inhibition experiments using PK59 and KP4 cells, which were identified as PDAC cells having a wild *TP53* status by the open database.[24] At first, we silenced SETDB1 expression with short hairpin RNA in PK59 and KP4 cells. qRT-PCR analysis revealed decreased *SETDB1* expression and elevated *TP53* expression in SETDB1 silenced PK59 and KP4 cells (Figure 7*A*). We next developed orthotopic PDAC models using SETDB1 silenced PK59 cells. The tumor size was significantly smaller in SETDB1 silenced PK59 cells compared to controls (Figure 7*B*). In addition, qRT-PCR analysis revealed decreased *SETDB1* expression and elevated *TP53* expression in SETDB1 silenced orthotopic tumors (Figure 7*C*). Consistent with our mouse model data, these findings suggested that SETDB1 regulated TP53 expression in human PDAC cells and that decreased SETDB1 expression reduced the growth of human PDAC cells in vivo.

To provide further insights into how SETDB1 epigenetically regulates the expression of TP53, we next investigated whether SETDB1 regulates TP53 expression through H3K9me3 in human PDAC cells. Western blot analysis revealed that the expression of H3K9me3 was decreased in SETDB1 silenced PK59 cells compared to controls (Figure 7*D*). ChIP experiments revealed that the bindings of SETDB1 and H3K9me3 to *TP53* promoter regions were decreased in SETDB1 silenced PK59 cells compared to controls, respectively (Figure 7*E*). These data suggested that SETDB1 epigenetically regulated TP53 expression, at least in part, through H3K9me3 in human PDAC cells.

To further investigate the functional role of Setdb1 in pancreatic tumorigenesis, we also overexpressed *Setdb1* in 266-6 cells, which is a mouse pancreatic acinar cell line. The cell proliferation assay revealed that there were no significant differences between control and *Setdb1* overexpressed 266-6 cells (Supplementary Figure 9). This result suggested that overexpression of *Setdb1* did not affect cell proliferation in mouse pancreatic acinar cells.

Next, to further validate the effect of SETDB1 inhibition on growth of human PDAC cells, we performed growth inhibition experiments using mithramycin A, which is an antitumor antibiotic that suppresses *SETDB1* promoter activity and thereby inhibits the expression of SETDB1.[14,25] Our results revealed that the proliferation of PK59 cells was markedly inhibited by treatment with 500 nM of mithramycin A (Figure 7*F*). Immunostaining for cleaved caspase 3 and Annexin V/Ethidium Homodimer III, showed markedly increased number of apoptotic cells in PK59 cells treated with mithramycin A (Figure 7*F* and *G*). In addition, qRT-PCR analysis revealed decreased *SETDB1* expression and elevated *TP53* expression in PK59 and KP4 cells treated with mithramycin A (Figure 7*H*). Thus, mithramycin A inhibited proliferation of PDAC cells with up-regulating TP53-induced apoptosis. Therefore, consistent with our mouse data, these findings suggested that suppression of SETDB1 led to elevated TP53 expression and reduced growth of human PDAC cells. These data suggested that SETDB1 could be a therapeutic target for human PDAC.

Considering the limitation of orthotopic tumor models regarding human relevance, we further performed the bioinformatic analysis on human The Cancer Genome Atlas data. Analysis of The Cancer Genome Atlas data set of pancreatic cancer showed that PDAC cases with SETDB1 low expression retained at least 1 wild-type *TP53* allele less frequently (27% [4 of 15]) compared to PDAC cases with SETDB1 intermediate (53% [64 of 119]) and high (67% [10 of 15]) expression, respectively, which suggested that biallelic alterations in *TP53* alleles are required for the formation of PDAC with reduced SETDB1 expression also in human (Supplementary Figure 10). These data are consistent with results from our mouse experiments that *Setdb1* deletion protected against PDAC formation in the context of heterozygous *p53* deletion, but not homozygous *p53* deletion.

Discussion

In this study, we demonstrated that Setdb1 is required for PDAC formation by inhibiting apoptosis through the regulation of p53 expression in mice. First, we found that *Setdb1* deletion results in pancreatic atrophy concomitant

Figure 7. SETDB1 silencing led to elevated TP53 expression and reduced growth of human PDAC cells. (*A*) qRT-PCR analysis of *SETDB1* and *TP53* expression in PK59 and KP4 cells silenced with control and *SETDB1* short hairpin RNA (shRNA), respectively (n = 4). (*B*) Weight of orthotopic tumors derived from PK59 cells silenced with control and *SETDB1* shRNA, respectively (n = 3–4). (*C*) qRT-PCR analysis of *SETDB1* and *TP53* expression in orthotopic tumors derived from PK59 cells silenced with control and *SETDB1* shRNA, respectively (n = 3). (*D*) Western blot analysis for SETDB1 and H3K9me3 using PK59 cells silenced with control and *SETDB1* shRNA, respectively. (*E*) ChIP-qPCR of PK59 cells silenced with control and *SETDB1* shRNA, respectively, in the *TP53* promoter regions (n = 3). Means ± SEM are shown. Relative-fold enrichment of SETDB1 and H3K9me3 over IgG control. *Numbers* in primer names show distance from transcription start site. (*F*) Representative bright field images (*top row*) and immunostaining for cleaved caspase 3 (*green, middle row*) and co-immunostaining of E-cadherin (*red, bottom row*) counterstaining with 4′,6-diamidino-2-phenylindole (DAPI) (*blue*) in PK59 cells treated with dimethyl sulfoxide (DMSO) and 500 nM of mithramycin for 3 days (n = 3). Scale bar: 100 μm. (*G*) Representative immunostaining for Annexin V (*green*)/Ethidium Homodimer III (*red*) (*upper row*) and counterstaining with DAPI (*blue*) (*lower row*). (*H*) qRT-PCR analysis of *SETDB1* and *TP53* expression in PK59 and KP4 cells treated with DMSO and 500 nM of mithramycin A for 3 days, respectively (n = 3–4). **P* < .05; ***P* < .01; ****P* < .001, Student *t* test.

with a dramatic increase in apoptosis during pancreatic regeneration in response to cerulein-induced pancreatitis.

Second, we found that *Setdb1* deletion leads to up-regulated p53 expression and p53-induced apoptosis in the context of pancreatitis and PDAC initiation in mouse models. Notably, we revealed that *Setdb1* deletion protects against Kras-driven PDAC formation by inducing apoptosis in the context of heterozygous *p53* deletion. Furthermore, we showed that suppression of PDAC formation and increased apoptosis by *Setdb1* deletion are offset by homozygous *p53* deletion. In addition, mechanistically, we revealed that Setdb1 binds to the *p53* promoter regions to directly regulate its expression in mouse pancreatic acinar cells. These findings clearly demonstrated that Setdb1 is required for PDAC formation by inhibiting apoptosis through regulation of p53 expression in mice.

Third, consistent with our mouse data, we showed that suppression of SETDB1 leads to the elevated TP53 expression and reduces growth of human PDAC cells having a wild *TP53* status in the orthotopic tumor models. We also showed that SETDB1 epigenetically regulates TP53 expression, at least in part, through H3K9me3 in human PDAC cells. This finding is also supported by our inhibitor experiments in human PDAC cells, showing that suppression of SETDB1 in human *TP53* wild-type PDAC cells led to up-regulated TP53 expression and increased apoptosis. Consistent with our findings, recent reports have shown that silencing SETDB1 in non–small cell lung cancer cell lines increased TP53 expression and that SETDB1 was enriched in the *TP53* promoter regions in colon cancer cells.[12,20] Therefore, SETDB1 could be a therapeutic target for PDAC, which retains TP53 function. Although we showed that SETDB1 could be a therapeutic target for PDAC with normal TP53 function in this study, the role of SETDB1 in *TP53* mutated PDAC remains unclear. Therefore, further studies are crucial to clarify the role of SETDB1 in *TP53* mutated PDAC.

Fourth, we revealed that *Setdb1* deletion accelerated the formation of ADM and PanIN. Our data suggested that Setdb1 plays a tumor-suppressive role in premalignant stages of PDAC formation. Given that Setdb1 forms complexes with various proteins and also methylates nonhistone proteins,[14,26–28] this context-dependent roles of Setdb1 in PDAC formation are most likely due to a wide range of target genes of Setdb1 at distinct stages of PDAC formation. It awaits further investigation to elucidate the underlying mechanism by which *Setdb1* deletion accelerates formation of premalignant ADM/PanIN lesions.

A previous report showed that SETDB1 overexpression is associated with mutant *p53* through demethylating p53 at K370.[13] Given that mutant *p53* was stabilized by p53K370me2 and acted in an oncogenic manner in liver,[13] we also investigated whether p53K370me2 is changed in the absence of Setdb1 in *KCS* mice. Immunostaining for p53K370me2 revealed that there were no significant differences in the number of p53K370me2-positive cells between *KC* and *KCS* pancreata at 4 and 20 weeks of ages, respectively, suggesting that Setdb1 was not associated with p53K370me2 in pancreatic tumorigenesis in our mouse model (Supplementary Figure 11*A* and *B*).

In conclusion, we demonstrated that *Setdb1* deletion protects against PDAC formation by inducing p53-mediated apoptosis, revealing an essential role of Setdb1 in PDAC formation in mice. Furthermore, mechanistically, we showed that Setdb1 binds to the *p53* promoter regions to directly regulate p53 expression in the pancreas. Thus, although future studies are required to clarify the role of Setdb1 in *p53* mutated PDAC, Setdb1 could be a potential therapeutic target for PDAC.

Supplementary Material

Note: To access the supplementary material accompanying this article, visit the online version of *Gastroenterology* at www.gastrojournal.org, and at https://doi.org/10.1053/j.gastro.2020.04.047.

References

1. Ryan DP, Hong TS, Bardeesy N. Pancreatic adenocarcinoma. N Engl J Med 2014;371:1039–1049.
2. **De Carvalho DD, Sharma S**, You JS, et al. DNA methylation screening identifies driver epigenetic events of cancer cell survival. Cancer Cell 2012;21:655–667.
3. Kubicek S, O'Sullivan RJ, August EM, et al. Reversal of H3K9me2 by a small-molecule inhibitor for the G9a histone methyltransferase. Mol Cell 2007;25:473–481.
4. McCabe MT, Ott HM, Ganji G, et al. EZH2 inhibition as a therapeutic strategy for lymphoma with EZH2-activating mutations. Nature 2012;492:108–112.
5. Koutsioumpa M, Hatziapostolou M, Polytarchou C, et al. Lysine methyltransferase 2D regulates pancreatic carcinogenesis through metabolic reprogramming. Gut 2018;68:1271–1286.
6. **Mallen-St Clair J, Soydaner-Azeloglu R**, Lee KE, et al. EZH2 couples pancreatic regeneration to neoplastic progression. Genes Dev 2012;26:439–444.
7. Wang H, An W, Cao R, et al. mAM facilitates conversion by ESET of dimethyl to trimethyl lysine 9 of histone H3 to cause transcriptional repression. Mol Cell 2003;12:475–487.
8. Schultz DC, Ayyanathan K, Negorev D, et al. SETDB1: a novel KAP-1-associated histone H3, lysine 9-specific methyltransferase that contributes to HP1-mediated silencing of euchromatic genes by KRAB zinc-finger proteins. Genes Dev 2002;16:919–932.
9. Koide S, Oshima M, Takubo K, et al. Setdb1 maintains hematopoietic stem and progenitor cells by restricting the ectopic activation of nonhematopoietic genes. Blood 2016;128:638–649.
10. **Matsui T, Leung D**, Miyashita H, et al. Proviral silencing in embryonic stem cells requires the histone methyltransferase ESET. Nature 2010;464:927–931.

11. **Ceol CJ, Houvras Y**, Jane-Valbuena J, et al. The histone methyltransferase SETDB1 is recurrently amplified in melanoma and accelerates its onset. Nature 2011; 471:513–517.
12. Sun QY, Ding LW, Xiao JF, et al. SETDB1 accelerates tumourigenesis by regulating the WNT signalling pathway. J Pathol 2015;235:559–570.
13. Fei Q, Shang K, Zhang J, et al. Histone methyltransferase SETDB1 regulates liver cancer cell growth through methylation of p53. Nat Commun 2015;6:8651.
14. Wong CM, Wei L, Law CT, et al. Up-regulation of histone methyltransferase SETDB1 by multiple mechanisms in hepatocellular carcinoma promotes cancer metastasis. Hepatology 2016;63:474–487.
15. Xiao JF, Sun QY, Ding LW, et al. The c-MYC-BMI1 axis is essential for SETDB1-mediated breast tumourigenesis. J Pathol 2018;246:89–102.
16. **Witkiewicz AK, McMillan EA, Balaji U**, et al. Whole-exome sequencing of pancreatic cancer defines genetic diversity and therapeutic targets. Nat Commun 2015;6:6744.
17. Kawaguchi Y, Cooper B, Gannon M, et al. The role of the transcriptional regulator Ptf1a in converting intestinal to pancreatic progenitors. Nat Genet 2002;32:128–134.
18. Jackson EL, Willis N, Mercer K, et al. Analysis of lung tumor initiation and progression using conditional expression of oncogenic K-ras. Genes Dev 2001; 15:3243–3248.
19. Jensen JN, Cameron E, Garay MV, et al. Recapitulation of elements of embryonic development in adult mouse pancreatic regeneration. Gastroenterology 2005; 128:728–741.
20. **Chen K, Zhang F**, Ding J, et al. Histone methyltransferase SETDB1 promotes the progression of colorectal cancer by inhibiting the expression of TP53. J Cancer 2017;8:3318–3330.
21. **Yuan P, Han J**, Guo G, et al. Eset partners with Oct4 to restrict extraembryonic trophoblast lineage potential in embryonic stem cells. Genes Dev 2009; 23:2507–2520.
22. Evan GI, Hah N, Littlewood TD, et al. Re-engineering the pancreas tumor microenvironment: a "regenerative program" hacked. Clin Cancer Res 2017;23:1647–1655.
23. **Sodir NM, Kortlever RM**, Barthet VJA, **Campos T**, et al. Myc instructs and maintains pancreatic adenocarcinoma phenotype. Cancer Discov 2020;10:588–607.
24. Giacomelli AO, Yang X, Lintner RE, et al. Mutational processes shape the landscape of TP53 mutations in human cancer. Nat Genet 2018;50:1381–1387.
25. Ryu H, Lee J, Hagerty SW, et al. ESET/SETDB1 gene expression and histone H3 (K9) trimethylation in Huntington's disease. Proc Natl Acad Sci U S A 2006; 103:19176–19181.
26. **Wang G, Long J, Gao Y**, et al. SETDB1-mediated methylation of Akt promotes its K63-linked ubiquitination and activation leading to tumorigenesis. Nat Cell Biol 2019;21:214–225.
27. Guo J, Dai X, Laurent B, et al. AKT methylation by SETDB1 promotes AKT kinase activity and oncogenic functions. Nat Cell Biol 2019;21:226–237.
28. Hamamoto R, Saloura V, Nakamura Y. Critical roles of non-histone protein lysine methylation in human tumorigenesis. Nat Rev Cancer 2015;15:110–124.

Author names in bold designate shared co-first authorship.

Received July 8, 2019. Accepted April 18, 2020.

Correspondence
Address correspondence to: Akihisa Fukuda, MD, PhD, Department of Gastroenterology and Hepatology, Kyoto University Graduate School of Medicine, 54 Shogoin-Kawahara-cho, Sakyo-ku, Kyoto 606-8507, Japan. e-mail: fukuda26@kuhp.kyoto-u.ac.jp; fax: +81-75-753-4303.

Acknowledgments
The authors thank Yoshiya Kawaguchi for sharing *Ptf1a*^{Cre} mice, David Tuveson for sharing *Kras*^{G12D} mice, Yoichi Shinkai for sharing *Setdb1*$^{f/f}$ mice, and Kei Fukuda for helpful advices and all members of the Fukuda laboratory for technical assistance and helpful discussions. Covaris S220 and GeneSpring were performed at the Medical Research Support Center, Graduate School of Medicine, Kyoto University, which was supported by Platform for Drug Discovery, Informatics, and Structural Life Science from the Ministry of Education, Culture, Sports, Science and Technology, Japan.

Transcript Profiling: All original microarray data were deposited in the Gene Expression Omnibus at National Center for Biotechnology Information (GSE 145775).

CRediT Authorship Contributions
Satoshi Ogawa, MD (Conceptualization: Lead; Data curation: Lead; Formal analysis: Lead; Investigation: Lead; Writing – original draft: Lead; Writing – review & editing: Lead). Akihisa Fukuda, MD, PhD (Conceptualization: Equal; Data curation: Equal; Formal analysis: Equal; Funding acquisition: Lead; Project administration: Lead; Resources: Lead; Writing – original draft: Supporting; Writing – review & editing: Lead). Yoshihide Matsumoto, MD (Investigation: Supporting). Yuta Hanyu, Medical Student (Investigation: Supporting). Makoto Sono, MD (Investigation: Supporting). Yuichi Fukunaga, PharmD (Investigation: Supporting). Tomonori Masuda, MD (Investigation: Supporting). Osamu Araki, MD (Investigation: Supporting). Munemasa Nagao, MD (Investigation: Supporting). Takaaki Yoshikawa, MD (Investigation: Supporting). Norihiro Goto, MD, PhD (Investigation: Supporting). Yukiko Hiramatsu, MD, PhD (Data curation: Supporting; Investigation: Supporting). Motoyuki Tsuda, MD, PhD (Data curation: Supporting; Investigation: Supporting; Writing – review & editing: Supporting). Takahisa Maruno, MD (Investigation: Supporting). Yuki Nakanishi, MD, PhD (Data curation: Supporting; Investigation: Supporting; Writing – review & editing: Supporting). Mohammed Salah Hussein, MD, PhD (Investigation: Supporting). Tatsuaki Tsuruyama, MD, PhD (Data curation: Supporting).

Conflicts of interest
This author discloses the following: Yuichi Fukunaga is employed by Sumitomo Dainippon Pharma. The remaining authors disclose no conflicts.

Funding
This work was supported in part by Grants-in-Aid KAKENHI (JP25112707, JP26293173, JP14J03460, JP16K09394, JP16K15427, and JP17J055511), a research program as part of the Project for Development of Innovative Research on Cancer Therapeutics (P-Direct) from the Ministry of Education, Culture, Sports, Science, and Technology and the Japan Society for the Promotion of Science. It was also supported by Japan Agency for Medical Research and Development, the Project for Cancer Research and Therapeutic Evolution (JP18cm0106142h0001) and AMED-PRIME (JP17cm0106XXXh0001). It was also supported by Princess Takamatsu Cancer Research Fund (13-24514, 17-24924), the Mochida Foundation (2017bvAg), the Mitsubishi Foundation (281119), the Uehara Foundation (201720143), and the Takeda Foundation (201749741).

Supplementary Materials and Methods

Immunohistochemistry

Mouse tissues were fixed overnight in 4% paraformaldehyde, dehydrated with 70% ethanol, embedded in paraffin, and cut into 5-μm sections. Paraffin-embedded sections were stained with H&E, or Sirius Red staining (saturated picric acid containing 0.1% Direct Red 80 and 0.1% Fast Green FCF; Sigma-Aldrich). For immunohistochemistry, antigen retrieval was performed by incubating the sections in 10 mM citric acid buffer (pH 6.0) or EDTA buffer (pH 8.0) for 15 minutes at 98°C. Blocking was performed by incubating sections with blocking solution (Dako, Santa Clara, CA; catalog no. X0909). For primary antibodies, the incubation was performed overnight at 4°C or 2 hours at room temperature in a humidified chamber. Secondary antibody incubation was performed for 1 hour at room temperature. Immunoperoxidase labeling was performed with ABC Kit (Vector Laboratories, Burlingame, CA; catalog no. PK-6102). The sections were then colored with diaminobenzidine substrate (Dako, catalog no. K3468) and were counterstained with hematoxylin. For immunofluorescence, sections were incubated with primary antibody overnight at 4°C or 2 hours at room temperature. The sections were then incubated with fluorescence-conjugated secondary antibody (Invitrogen, Carlsbad, CA) for 1 hour at room temperature. Primary antibodies are listed in Supplementary Table 1.

Terminal deoxynucleotidyl transferase–mediated deoxyuridine triphosphate nick-end labeling staining (*In Situ* Death Detection Kit, catalog no. 11 684 795 910; Roche, Basel, Switzerland) was performed to assess apoptotic cells. Claudin 18 staining was performed to assess the PanIN areas. Sirius Red staining was performed to visualize fibrotic areas. Annexin V/Ethidium Homodimer III staining (Apoptotic/Necrotic Cells Detection Kit, catalog no. PK-CA707-30017; Promocell, Heidelberg, Germany) was performed to assess the apoptotic and necrotic cells.

For quantitative analysis of PanIN or fibrotic areas, the measurement of Claudin 18–positive PanIN, or Sirius Red–positive areas was performed using ImageJ software (National Institutes of Health, Bethesda, MA). Three whole pancreas sections per mouse were analyzed. Whole pancreatic areas were measured using a BZ-X Analyzer (Keyence, Osaka, Japan). For quantitative analysis of cell numbers or scoring, counting was performed using 3 random high-power fields from 3 sections or 5 random high-power fields from one section. For pathology score of pancreatitis, we evaluated the severity of pancreatitis as described previously.[1] We evaluated the intensity of SETDB1 expression in human pancreatic cancer tissues immunohistochemically and scored it ranging from 0 to 3 (0 = none, 1 = low, 2 = medium, 3 = high). Scoring was performed by 2 blinded investigators and reviewed by a board-certified pathologist. The mean score was shown as a representative value of individual samples and the cutoff score was set at 2 to distinguish negative and positive SETDB1 expression.

Western Blot Analysis

Pancreatic tissues were homogenized in Cell Lysis Buffer (Cell Signaling Technology, Danvers, MA) supplemented with Protease Inhibitor Cocktail (Cell Signaling Technology). Tissues were separated by sodium dodecyl sulfate polyacrylamide gel electrophoresis and transferred to nitrocellulose membranes. After blocking, membranes were incubated with primary antibodies overnight at 4°C, followed by horseradish peroxidase–conjugated secondary antibodies. The immobilized peroxidase activity was detected with an enhanced chemiluminescence system (Pierce Western Blotting Substrates, Thermo Fisher Scientific). Primary antibodies are listed in Supplementary Table 1.

Methyltransferase Activity Quantification Assay

Nuclear extracts were prepared from pancreatic tissues using Nuclear Extraction Kit (ab113473; Abcam, Cambridge, UK) following the manufacturer's protocols. We quantified histone methyltransferase activity with these extracts using Histone Methyltransferase H3 (K9) Activity Quantification Assay Kit (ab113453; Abcam) following the manufacturer's protocols. The absorbance at 450 nm was measured using a plate reader. Methyltransferase activity was calculated by the following formula: activity [OD/h/mg] = (Sample OD – blank OD) / (protein amount [μg] $\times$ incubation hour).

RNA Isolation and Quantitative Reverse Transcription Polymerase Chain Reaction

Mouse pancreata were collected in RNAlater (Ambion, Austin, TX), and subsequently, total RNA was extracted using the RNA mini Kit (Qiagen, Hilden, Germany). Single-strand complementary DNA (cDNA) was synthesized using a ReverTra Ace qPCR RT Kit (TOYOBO, Tokyo, Japan). qRT-PCR was performed using SYBR Green Master Mix (Roche Applied Science) and LightCycler 480 (Roche Applied Science). The expression levels were standardized by comparing to the levels of *Gapdh*. Primer sequences are listed in Supplementary Table 2.

Acinar Cell Isolation and Culture

Mouse pancreata were minced into small pieces and digested with Collagenase P (0.4 mg/mL) at 37°C for 10 minutes. After 2 washes with Hanks' Balanced Salt solution buffer containing 5% fetal bovine serum, the tissue suspension was filtered through a 100-μm cell strainer. The flow-through was layered onto Hanks' Balanced Salt solution plus 30% fetal bovine serum solution and centrifuged. The cell pellet was centrifuged and resuspended in a 1:1 ratio of acinar cultured media to rat-tail collagen Type I solution (1 mg/mL final collagen concentration), and plated onto a 24-well plate coated with rat-tail collagen Type I. Acinar cultured medium consisted of Waymouth's media supplemented with 10% fetal bovine serum, 1% penicillin/streptomycin, 100 μg/mL trypsin inhibitor, and 1 μg/mL dexamethasone.[2–4]

For quantitative analysis of ADM formation rate (percent of total cell clusters), cell clusters were seeded

in triplicate and were counted from at least 3 optical fields per well.

Microarray Analysis

The quality of RNA extracted from pancreata in *Ptf1a*^{Cre}; *Kras*^{G12D} and *Ptf1a*^{Cre}; *Kras*^{G12D}; *Setdb1*$^{f/f}$ mice was examined with an Agilent 2100 bioanalyzer (Agilent Technologies, Santa Clara, CA) and a Nanodrop (Thermo Fisher Scientific, Waltham, MA).

The RNA samples were hybridized using SurePrint G3 Mouse Gene Expression 8×60K v2 (Agilent Technologies). The raw data were normalized by GeneSpring GX 14.9 (Agilent Technologies). Unnamed genes were excluded. The gene expression data of the pancreata was analyzed using Gene Set Enrichment Analysis software and the Molecular Signature Database, which was provided by the Broad Institute of Massachusetts Institute of Technology and Harvard University.[5] The pathway analyses and Gene Ontology enrichment analyses of the gene expression data in 3000 most up-regulated genes were performed using DAVID 6.8.[6,7]

Chromatin Immunoprecipitation

ChIP was performed using Simple ChIP Plus Enzymatic Chromatin IP Kit (magnetic beads) (9005; Cell Signaling Technology). Briefly, isolated mouse acinar cells or human PDAC cells were crosslinked with 1% formaldehyde and incubated for 10 minutes with gentle shaking at room temperature. Crosslinking was stopped by addition of glycine for 5 minutes with gentle shaking. After washing by phosphate-buffered saline, fixed cells were lysed and subsequently sheared using Covaris S220 (Covaris, Woburn, MA), Sheared chromatin (1/50) was kept aside as input, and the remaining chromatin was immunoprecipitated with 1.5 μg rabbit IgG antibody (provided in kit), 2 μg anti-Setdb1 antibody (11231-1-AP; Proteintech Group, Rosemont, IL), and 1.5 μg anti-H3K9me3 antibody (ab8898; Abcam). Chromatin was collected using magnetic beads and de-crosslinked. The DNA was purified using DNA spin columns. Purified DNA was amplified by SYBR Green Master Mix (Roche). We used IgG antibody, which exhibited minimal binding to chromatin at all the promoter regions investigated, as negative control, and calculated the fold change. Fold enrichment over IgG was calculated based on percentage of input values (percent Input = $2\% \times 2^{(\text{C[T] 2\%Input Sample - C[T] IP Sample})}$) compared to negative control.

The primer sequences listed in Supplementary Table 2 were used for identification of putative binding sites of Setdb1 and H3K9me3 on *p53* promotor regions.

Vectors Transfection and Cell Proliferation Assay

To generate cells overexpressing Setdb1, Setdb1 expression vectors, pCAG-3×Flag-ESET-IRESbsd (gift from Y. Shinkai) were transfected into 266-6 cells with Lipofectamine 3000 (Invitrogen) following the manufacturer's protocols. Total RNA was extracted from 266-6 cells transfected with vectors for 3 days using RNA mini kit. For cell proliferation assay, 266-6 cells (1.0×10^4) were seeded in 96-well plates for 24 hours and transfected. Cell proliferation was evaluated using CellTiter 96 AQueous One Solution Cell Proliferation Assay (Promega, Madison, WI) following the manufacturer's protocol. The absorbance at 490 nm was measured using a plate reader. Background absorbance from empty wells was subtracted from that of sample wells.

Lentivirus Transduction and Infection of Pancreatic Cancer Cells

Silencing SETDB1 was achieved by using pLKO-shSETDB1 (SETDB1 MISSION shRNA SHCLND-NM_012432 TRCN0000276169 for PK59 cells and TRCN0000276105 for KP4 cells). To produce lentiviruses, HEK293T cells were transfected with the targeting plasmid, pCAG-HIVgp, and pCMV-VSV-G-RSV-Rev (kind gifts from Dr Hiroyuki Miyoshi, RIKEN BioResource Center, Tsukuba, Japan) plasmids. The culture supernatants were collected 48 hours after transfection, filtered, concentrated by PEG-it (System Biosciences, Palo Alto, CA; catalog no. LV810A-1) and resuspended in Hanks' Balanced Salt solution. Infection was performed in the presence of polybrene (5 μg/mL) overnight, followed by selection with puromycin. For orthotopic tumor model experiments, 6- to 8-week-old NOD/SCID mice (NOD.CB17-Prkdcscid/J) (purchase from Jackson Laboratory; JAX strain 001303) were used. Mice were administered intrapancreatic injections of PK59 cells (1.0×10^6) transfected with control and SETDB1 short hairpin RNA (shRNA) in 25 μL Matrigel + 25 μL medium. Mice were analyzed after 3 weeks.

The Cancer Genome Atlas Data Set Analysis

The Cancer Genome Atlas (Firehose legacy) data of 149 pancreatic cancer patients in terms of mutations, copy number alterations, and messenger RNA expression *Z* scores were obtained from cBioportal.[8,9] Cases with a mutation and a shallow deletion or cases with a deep deletion were considered as cases retaining no wild *TP53* by analyzing *TP53* mutations and copy number alterations. The rest of cases were considered as cases retaining at least 1 wild *TP53* allele. The cutoff SETDB1 expression was upper 10% for high, middle 80% for intermediate, and lower 10% for low.

Data Availability

All original microarray data were deposited in the Gene Expression Omnibus at National Center for Biotechnology Information (GSE 145775). The data that support the findings of this study are included in this article and its Supplementary Material or available from the corresponding author upon reasonable request.

References

1. Schmidt J, Rattner DW, Lewandrowski K, et al. A better model of acute pancreatitis for evaluating therapy. Ann Surg 1992;215:44–56.
2. **Shi G, DiRenzo D, Qu C**, et al. Maintenance of acinar cell organization is critical to preventing Kras-induced acinar-ductal metaplasia. Oncogene 2013;32:1950–1958.
3. Means AL, Meszoely IM, Suzuki K, et al. Pancreatic epithelial plasticity mediated by acinar cell trans-differentiation and generation of nestin-positive intermediates. Development 2005;132:3767–3776.
4. **Fukuda A, Wang SC**, Morris JPt, et al. Stat3 and MMP7 contribute to pancreatic ductal adenocarcinoma initiation and progression. Cancer Cell 2011;19:441–455.
5. **Subramanian A, Tamayo P**, Mootha VK, et al. Gene set enrichment analysis: a knowledge-based approach for interpreting genome-wide expression profiles. Proc Natl Acad Sci U S A 2005;102:15545–15550.
6. **Huang da W, Sherman BT**, Lempicki RA. Bioinformatics enrichment tools: paths toward the comprehensive functional analysis of large gene lists. Nucleic Acids Res 2009;37:1–13.
7. **Huang da W, Sherman BT**, Lempicki RA. Systematic and integrative analysis of large gene lists using DAVID bioinformatics resources. Nat Protoc 2009;4:44–57.
8. Gao J, Aksoy BA, Dogrusoz U, et al. Integrative analysis of complex cancer genomics and clinical profiles using the cBioPortal. Sci Signal 2013;6:pl1.
9. Cerami E, Gao J, Dogrusoz U, et al. The cBio cancer genomics portal: an open platform for exploring multidimensional cancer genomics data. Cancer Discov 2012;2:401–404.

Author names in bold designate shared co-first authorship.

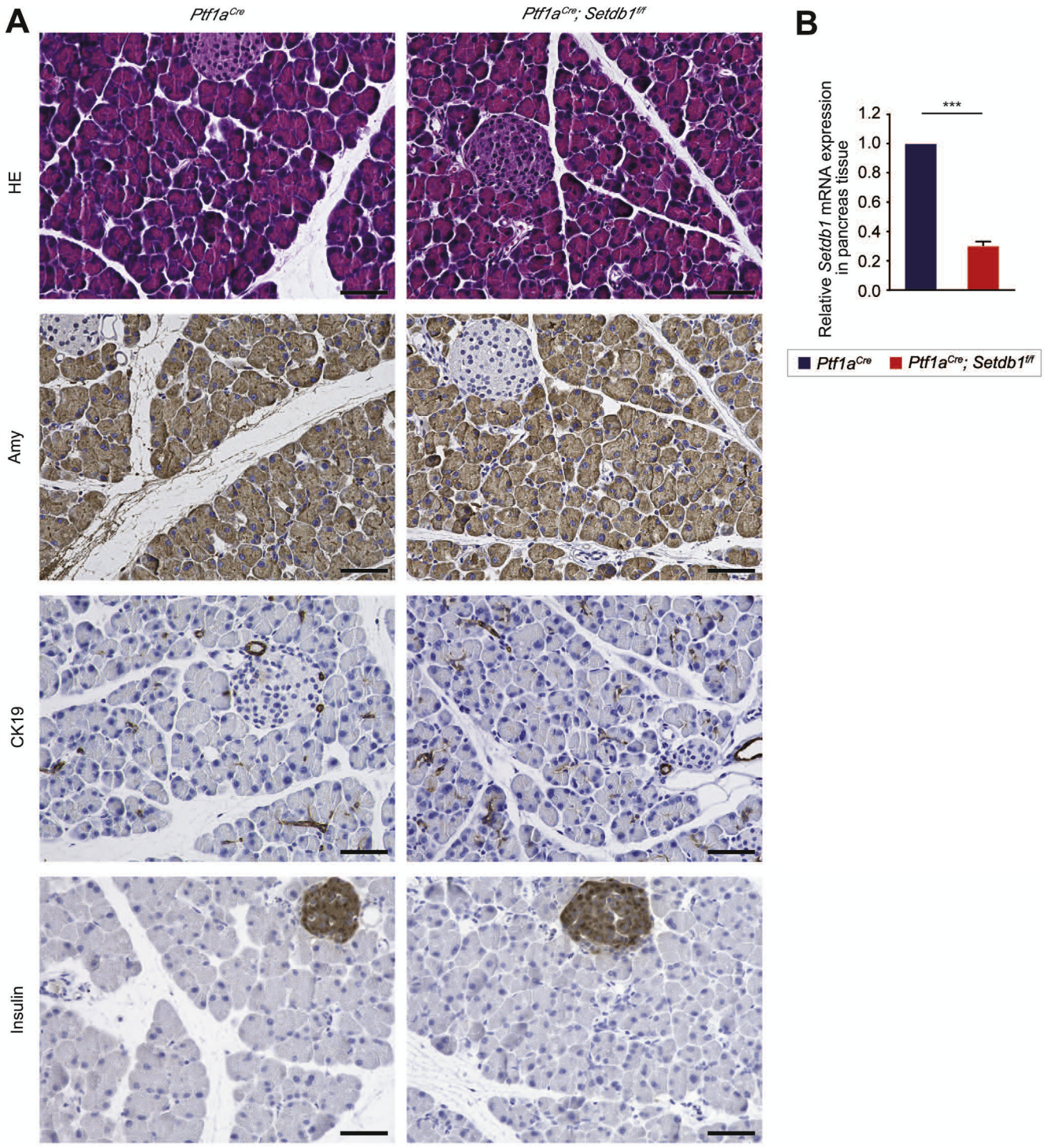

Supplementary Figure 1. Setdb1 was dispensable for pancreatic development. (*A*) Representative H&E staining and immunostaining for amylase, CK19, and insulin at 6 weeks of age in *Ptf1a*^{Cre} and *Ptf1a*^{Cre} *Setdb1*$^{f/f}$ mice (n = 3). Scale bars: 50 μm. (*B*) qRT-PCR analysis of *Setdb1* in *Ptf1a*^{Cre} and *Ptf1a*^{Cre}*; Setdb1*$^{f/f}$ pancreata (n = 3). Means ± SEM are shown. **P* < .05; ***P* < .01; ****P* < .001, Student *t* test.

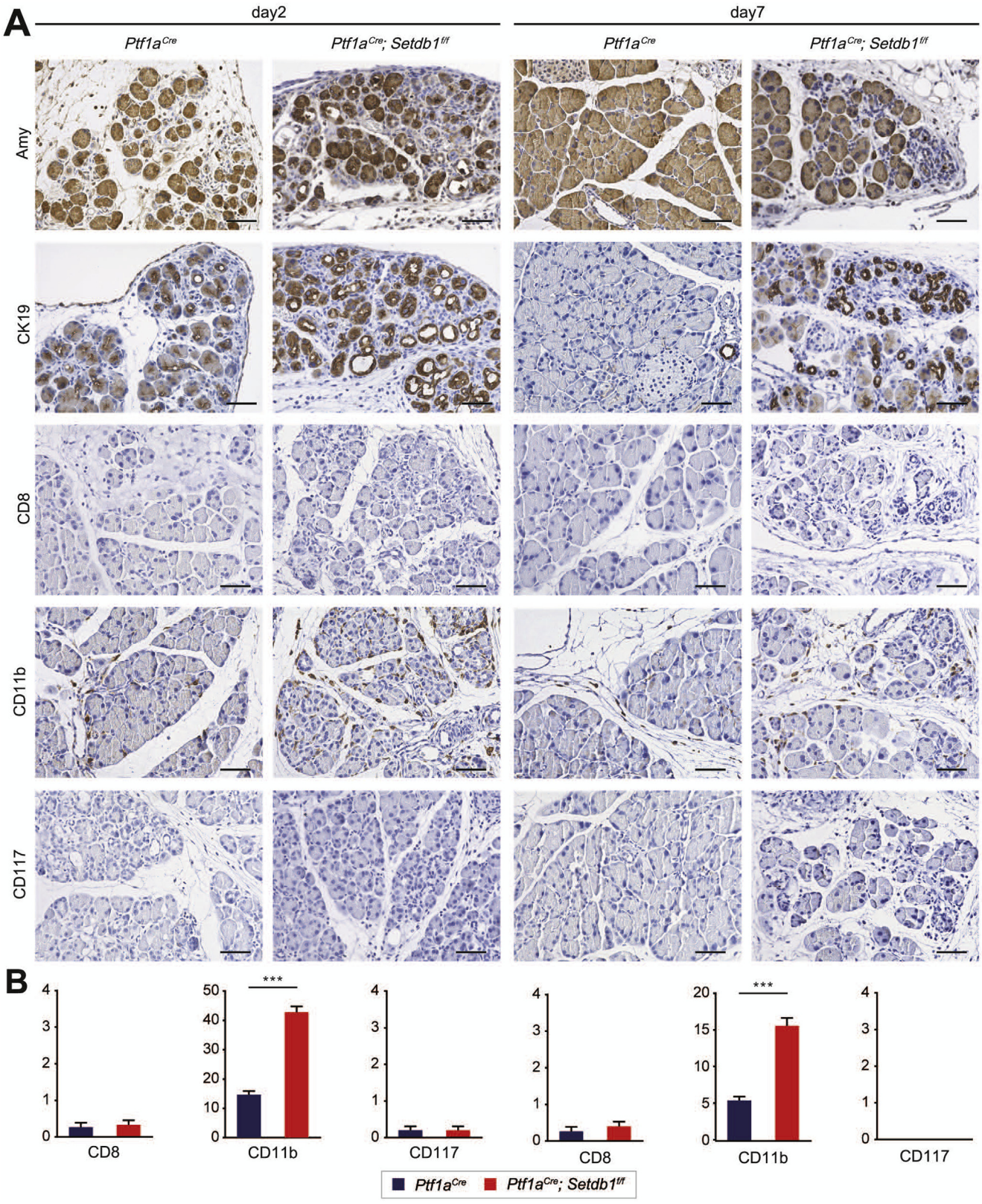

Supplementary Figure 2. Characteristics of inflammatory cells in cerulein-induced pancreatitis in *Ptf1a^{Cre}; Setdb1$^{f/f}$* mice. (*A*) Representative immunostaining for amylase, CK19, CD8, CD11b, and CD117 in *Ptf1a^{Cre}* and *Ptf1a^{Cre}; Setdb1$^{f/f}$* mice 2 days after cerulein treatment (*left 2 rows*) (n = 3) and 7 days after cerulein treatment (*right 2 rows*) (n = 3). Scale bars: 50 μm. (*B*) Numbers of CD8-, CD11b-, and CD117-positive cells/high-power field (HPF) in *Ptf1a^{Cre}* and *Ptf1a^{Cre}; Setdb1$^{f/f}$* mice 2 days (*left 3 graphs*) and 7 days (*right 3 graphs*) after cerulein treatment (n = 3). Means ± SEM are shown.

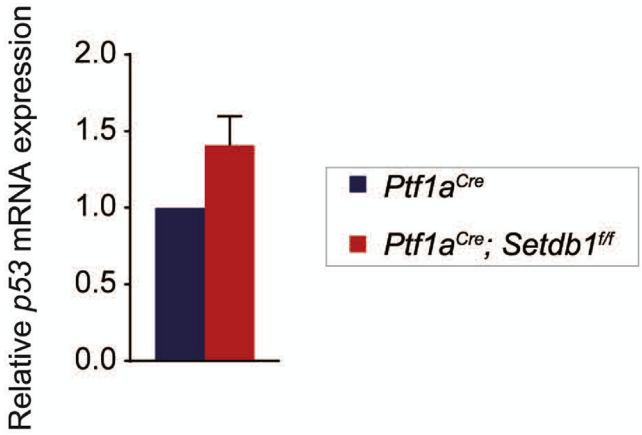

Supplementary Figure 3. *p53* expression was comparable between *Ptf1a*^{Cre} and *Ptf1a*^{Cre}*; Setdb1*$^{f/f}$ pancreata in a physiological condition. qRT-PCR analysis of *p53* expression in *Ptf1a*^{Cre} and *Ptf1a*^{Cre}*; Setdb1*$^{f/f}$ pancreata at 6 weeks of age (n = 4). Means ± SEM are shown. **P* < .05; ***P* < .01; ****P* < .001, Student *t* test. mRNA, messenger RNA.

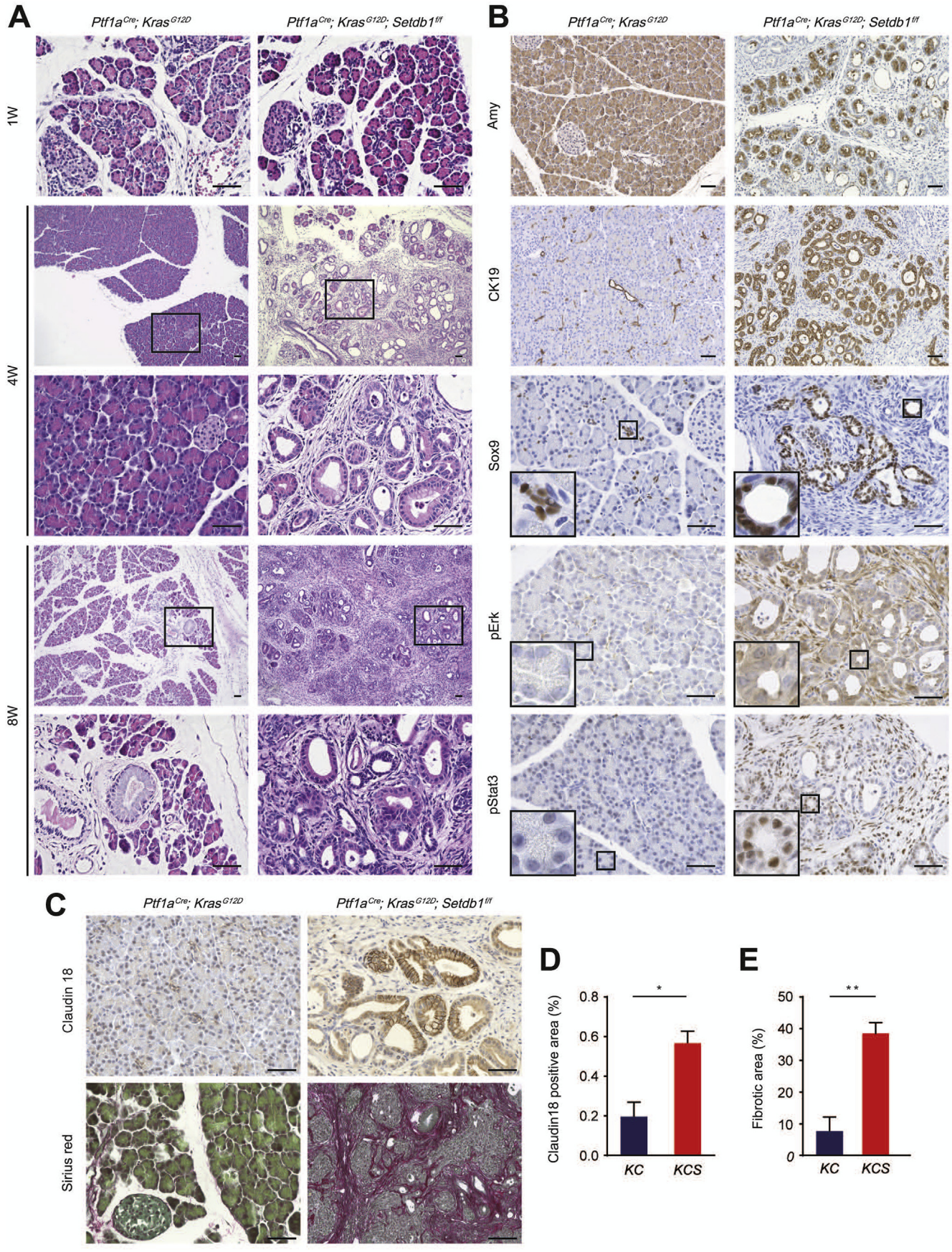
A
Ptf1a^Cre; Kras^G12D
Ptf1a^Cre; Kras^G12D; Setdb1^f/f
1W
4W
8W
B
Ptf1a^Cre; Kras^G12D
Ptf1a^Cre; Kras^G12D; Setdb1^f/f
Amy
CK19
Sox9
pErk
pStat3
C
Ptf1a^Cre; Kras^G12D
Ptf1a^Cre; Kras^G12D; Setdb1^f/f
Claudin 18
Sirius red
D
Claudin18 positive area (%)
0.8
0.6
0.4
0.2
0.0
*
KC
KCS
E
Fibrotic area (%)
50
40
30
20
10
0
**
KC
KCS

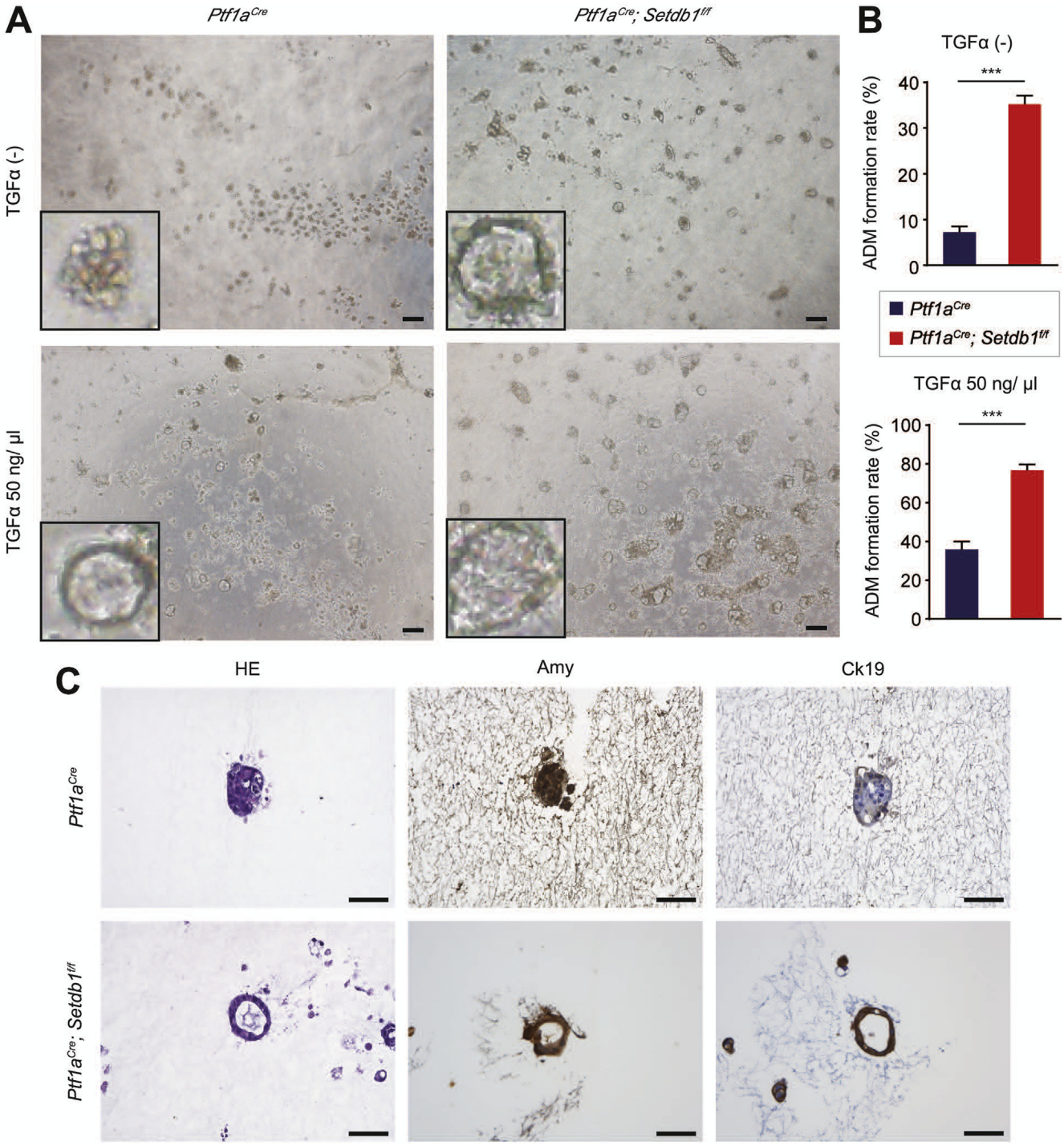

Supplementary Figure 5. *Setdb1*-null acinar cells converted to ADM in a cell-autonomous manner ex vivo. (*A*) Representative bright field images of acinar cell clusters from *Ptf1a*^{Cre} and *Ptf1a*^{Cre}*; Setdb1*$^{f/f}$ mice at 6 weeks of age after 2 days of culture in collagen gel without transforming growth factor–α (TGFα) (*upper row*) and with TGFα (*lower row*) (n = 3). Scale bars: 200 μm. (*B*) Quantification of ductal cystic structures in 3-dimensional (3D) cultured acinar cell clusters from *Ptf1a*^{Cre} and *Ptf1a*^{Cre} *Setdb1*$^{f/f}$ mice at 6 weeks of age after 2 days of culture in collagen gel without TGFα (*b*) and with TGFα (*c*) (n = 3). Means ± SEM are shown. (*C*) Representative H&E staining and immunostaining for amylase (Amy) and CK19 in 3D-cultured acinar cell clusters from *Ptf1a*^{Cre} and *Ptf1a*^{Cre} *Setdb1*$^{f/f}$ mice at 6 weeks of age after 2 days of culture in collagen gel without TGFα. Scale bars: 50 μm. *$P < .05$; **$P < .01$; ***$P < .001$, Student *t* test.

Supplementary Figure 4. *Setdb1* deletion markedly accelerated the formation of Kras-driven premalignant ADM/PanIN lesions. (*A*) Representative H&E staining at 1, 4, and 8 weeks of age in *KC* and *KCS* mice (n = 3–5). Scale bars: 50 μm. (*B*) Representative immunostaining for amylase (Amy), CK19, sex determining region Y box 9 (Sox9), phosphorylated extracellular signal–regulated kinase (pErk), and phosphorylated signal transducer and activator of transcription 3(pStat3) in *KC* and *KCS* mice at 4 weeks of age (n = 3). Scale bars: 50 μm. (*C*) Representative immunostaining for Claudin 18 (*upper row*), and Sirius Red staining (*lower row*) in *KC* and *KCS* mice at 4 weeks of age (n = 3). Scale bars: 50 μm. (*D, E*) Quantification of Claudin 18–positive (*D*) and fibrotic (*E*) area in *KC* and *KCS* pancreata (n = 3). Means ± SEM are shown. *$P < .05$; **$P < .01$; ***$P < .001$, Student *t* test.

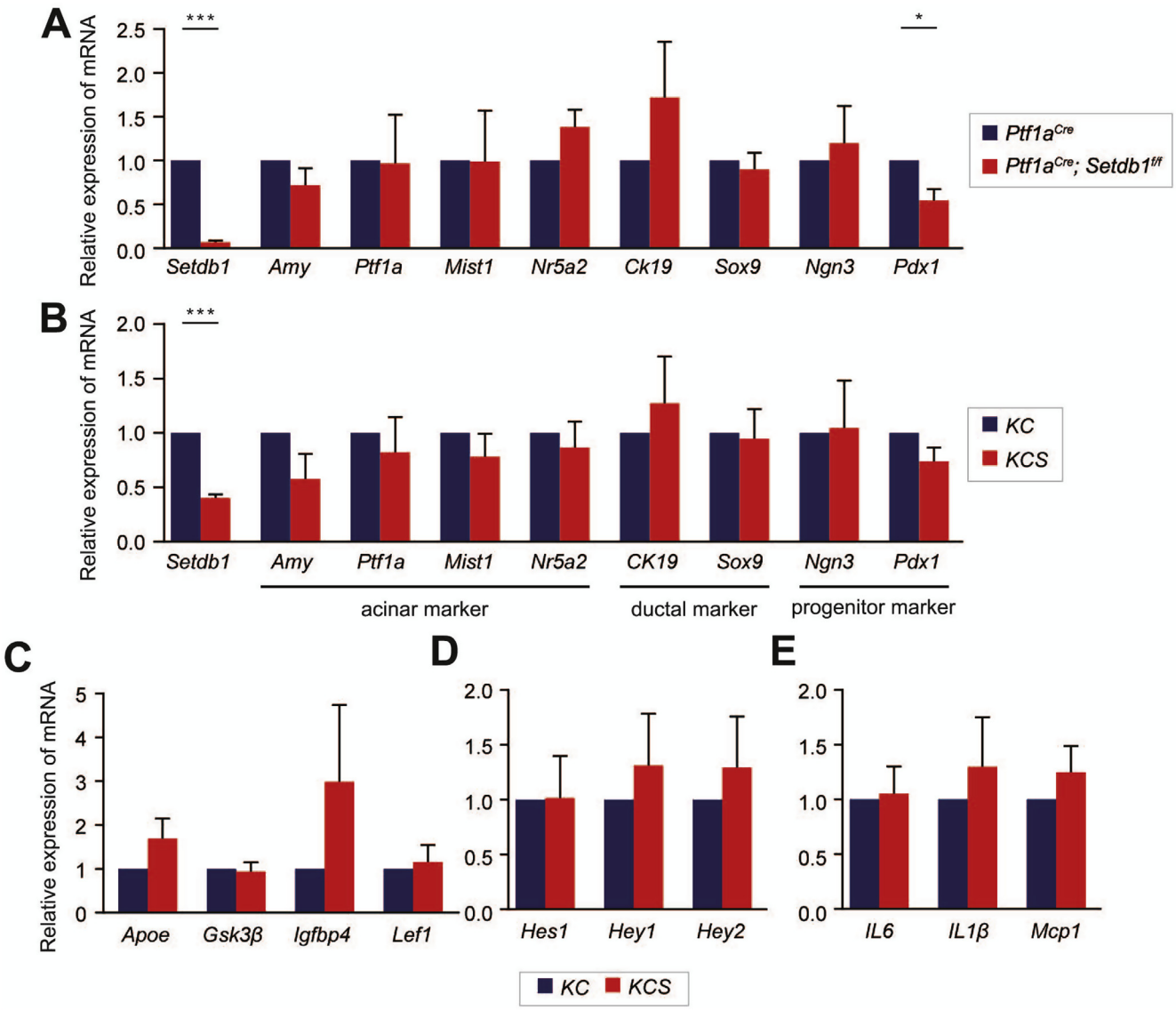

Supplementary Figure 6. *Setdb1* deletion did not alter the expression of pancreatic transcription factors, Wnt pathway, Notch pathway, and inflammation. (*A*) qRT-PCR analysis of pancreatic transcription factors of acinar cells isolated from *Ptf1a*^{Cre} and *Ptf1a*^{Cre} *Setdb1*$^{f/f}$ mice at 6weeks of age (n = 3). (*B*) qRT-PCR analysis of pancreatic transcription factors of *KC* and *KCS* pancreata at 1 week of age (n = 3). (*C, D, E*) qRT-PCR analysis of mediators related to Wnt pathway (*C*), Notch pathway (*d*) and inflammation (*e*) of *KC* and *KCS* pancreata at 1 week of age (n = 3). *$P < .05$; **$P < .01$; ***$P < .001$, Student *t* test.

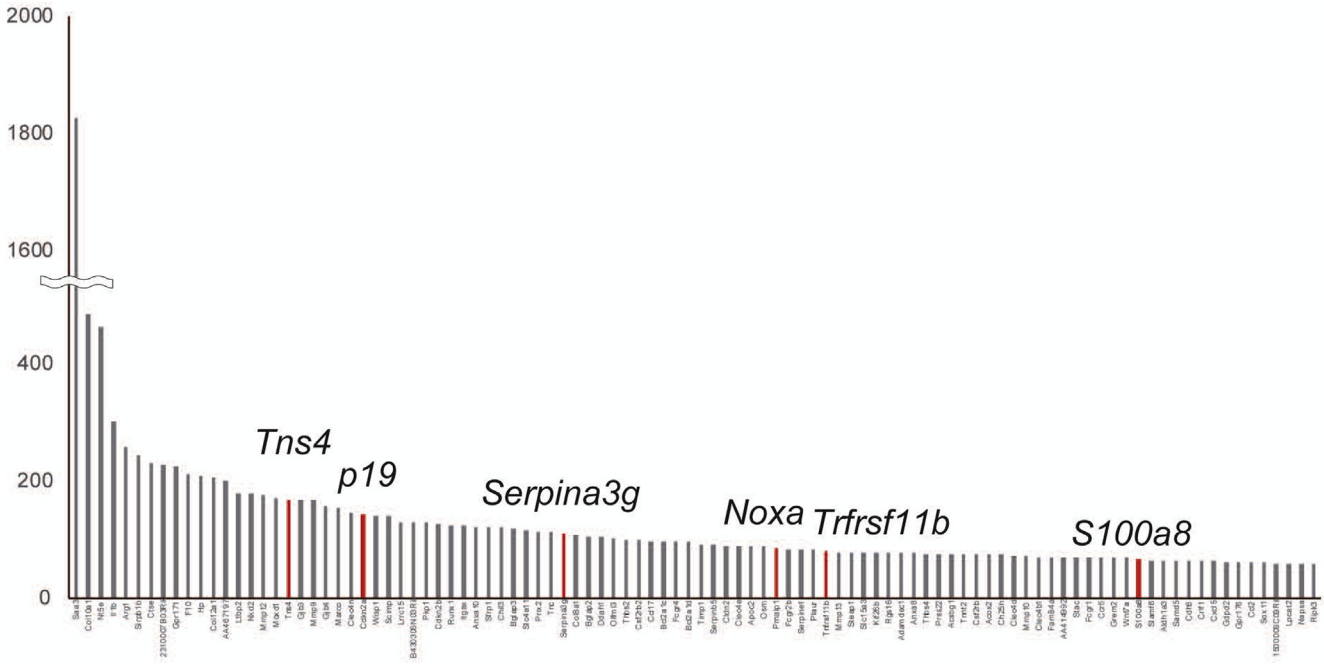

Supplementary Figure 7. Genes related to apoptosis were among the 100 most up-regulated genes in *KCS* mice. One hundred most up-regulated genes identified by microarray analysis in *KCS* pancreata compared with *KC* pancreata. The *red bars* show the factors involved in apoptosis.

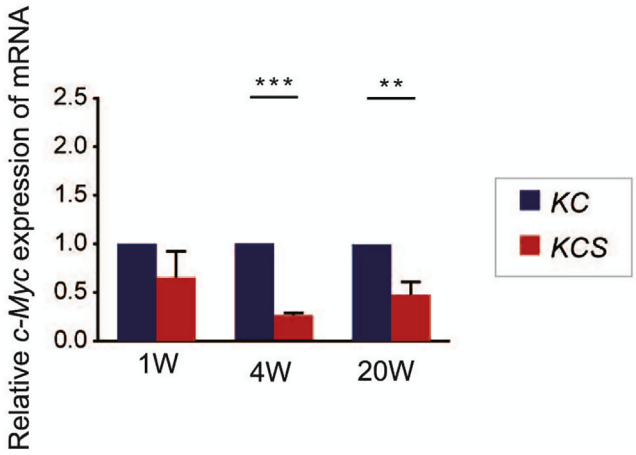

Supplementary Figure 8. The RAS-MYC oncogenic axis tended to be down-regulated in *KCS* mice compared to *KC* mice. qRT-PCR analysis of *c-Myc* expression in *KC* and *KCS* mice at 1, 4, and 20 weeks of age (n = 3, respectively). Means ± SEM are shown. *$P < .05$; **$P < .01$; ***$P < .001$, Student *t* test.

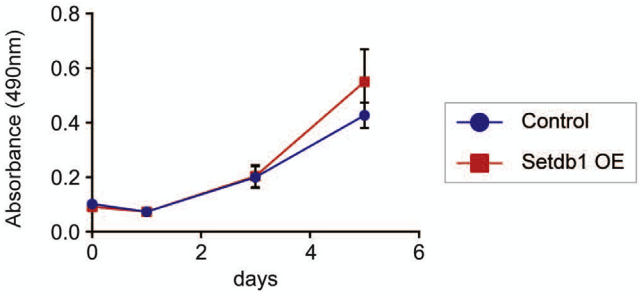

Supplementary Figure 9. There were no significant differences in terms of cell proliferation between control and *Setdb1* overexpressed mouse pancreatic acinar cells. Cell proliferation assay of control and *Setdb1* overexpressed 266-6 cells (n = 3). *$P < .05$; **$P < .01$; ***$P < .001$, Student *t* test.

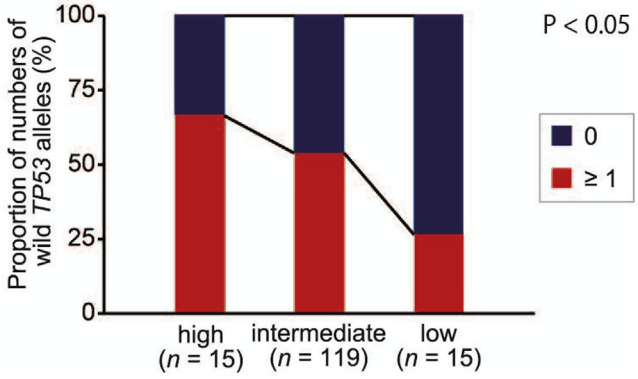

Supplementary Figure 10. Analysis of numbers of wild *TP53* alleles in PDAC patients with high, intermediate, low *SETDB1* expression using The Cancer Genome Atlas (TCGA) data set. Proportion of numbers of wild *TP53* alleles in PDAC patients with high, intermediate, and low expression of *SETDB1* in TCGA data set. The number of wild *TP53* alleles in cases retaining at least 1 wild *TP53* allele was described as ≥1, and that of wild *TP53* alleles in cases retaining no wild *TP53* alleles was described as 0. Cochran-Armitage test

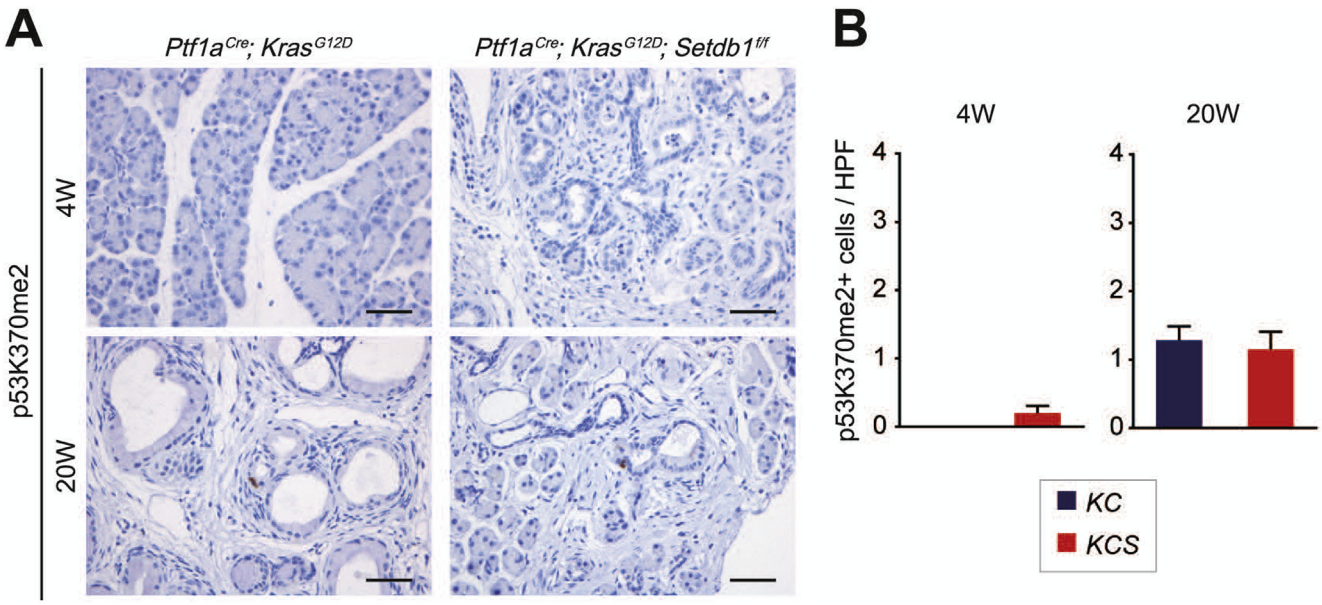

Supplementary Figure 11. There were no significant differences in the expression of P53K370me2 between *KC* and *KCS* mice. (*A*) Representative immunostaining for P53K370me2 in *KC* and *KCS* mice at 4 and 20 weeks of age (n = 3). (*B*) Numbers of P53K370me2–positive cells in *KC* and *KCS* at 4 and 20 weeks of age (n = 3). **P* < .05; ***P* < .01; ****P* < .001, Student *t* test.

Supplementary Table 1. Primary Antibodies for Immunohistochemistry and Western Blot Analysis

Antibodies	Source	Catalog no.	Dilution
Immunohistochemistry			
Setdb1	Cell Applications	CY1112	1:1000
Setdb1	Cell Applications	CP10377	1:500
Amylase	Abcam	ab21156	1:300
CK19	Abcam	ab52625	1:200
Insulin	Abcam	ab7842	1:100
F4/80	Abcam	ab6640	1:200
CD45	B & D	55039	1:50
CD3	Abcam	ab11089	1:100
CD8	B & D	550281	1:100
CD11b	Abcam	ab133357	1:4000
CD117	B & D	553352	1:200
Ki67	Biolegend	16A8	1:100
Cleaved caspase 3	Cell Signaling	9664S	1:500
E-cadherin	B & D	610182	1:100
p53	Vector Laboratories	VP-p956	1:500
Sox9	Chemicon	ab5535	1:10000
pErk	Cell Signaling	4370	1:200
pStat3	Cell Signaling	9145	1:200
Claudin 18	Invitrogen	700178	1:200
p53K370me2	St John's Laboratory	STJ90115	1:100
Western blot analysis			
Setdb1	Proteintech	11231-1-AP	1:2000
H3K9me3	Abcam	ab8898	1:5000
H3	Cell Signaling	9715	1:1000

pErk, phosphorylated extracellular signal–regulated kinase; pStat3, phosphorylated signal transducer and activator of transcription 3; Sox 9, sex determining region Y box 9.

Supplementary Table 2. Primer Sets for Quantitative Reverse Transcription Polymerase Chain Reaction Analyses and Chromatin Immunoprecipitation Experiments

Gene symbol	Forward	Reverse
Mouse		
Gapdh	AGGTCGGTGTGAACGGATTTG	TGTAGACCATGTAGTTGAGGTCA
p53	GTCACAGCACATGACGGAGG	TCTTCCAGATGCTCGGGATAC
Apaf1	AGTAATGGGTCCTAAGCATGTTG	GCGATTGGGAAAATCACGTAAAA
Noxa	GCAGAGCTACCACCTGAGTTC	CTTTTGCGACTTCCCAGGCA
Bcl2	GGGAGAACAGGGTATGATAACCG	TAGCCCCTCTGTGACAGCTTA
Setdb1	TGGCAACAGCGGTTCAGA	CAGAAGTTATCATCAGAGCTGTCATCA
Amy	TTGCCAAGGAATGTGAGCGAT	CCAAGGTCTTGATGGGTTATGAA
Ptf1a	TCCCATCCCCTTACTTTGATGA	GTAGCAGTATTCGTGTAGCTGG
Mist1	GCTGACCGCCACCATACTTAC	TGTGTAGAGTAGCGTTGCAGG
Nr5a2	TGTGTGGCGATAAAGTGTCTG	TCGACAGTAGGGACATCGTTT
Ck19	GGGGGTTCAGTACGCATTGG	GAGGACGAGGTCACGAAGC
Sox9	AGTACCCGCATCTGCACAAC	ACGAAGGGTCTCTTCTCGCT
Ngn3	AGTGCTCAGTTCCAATTCCAC	CGGCTTCTTCGCTTTTTGCTG
Pdx1	TTCCCGAATGGAACCGAGC	GCGTGAGCTTTGGTGGATT
Apoe	CTGACAGGATGCCTAGCCG	CGCAGGTAATCCCAGAAGC
Gsk3β	ATGGCAGCAAGGTAACCACAG	TCTCGGTTCTTAAATCGCTTGTC
Igfbp4	AGAAGCCCCTGCGTACATTG	TTGTTGGGATGTTCGCTCTCA
Lef1	TGTTTATCCCATCACGGGTGG	CATGGAAGTGTCGCCTGACAG
Hes1	ATAGCTCCCGGCATTCCAAG	GCGCGGTATTTCCCCAACA
Hey1	CCGACGAGACCGAATCAATAAC	TCAGGTGATCCACAGTCATCTG
Hey2	AAGCGCCCTTGTGAGGAAAC	GGTAGTTGTCGGTGAATTGGAC
IL6	TAGTCCTTCCTACCCCAATTTCC	TTGGTCCTTAGCCACTCCTTC
IL1β	GCAACTGTTCCTGAACTCAACT	TTGGTCCTTAGCCACTCCTTC
Mcp1	TTAAAAACCTGGATCGGAACCAA	GCATTAGCTTCAGATTTACGGGT
cMyc	TCTCCATCCTATGTTGCGGTC	TCCAAGTAACTCGGTCATCATCT
Human		
GAPDH	ATGGGGAAGGTGAAGGTCG	GGGGTCATTGATGGCAACAATA
SETDB1	GACTACAATACCGGGACAGTAGC	CCCAGCATCACCTGAATCAAT
TP53	CAGCACATGACGGAGGTTGT	CCAGACCATCGCTATCTGAGC

Name	Forward	Reverse
Mouse		
p53 (-1423bp)	AGGCACCGGTTCAAAGTCTG	AGAATGAAGACGTCGGAGGAG
p53 (-1144bp)	GAACGAGTGTCCAAAGCCAAG	GTGTAGGCAAAGTCGTTCCTTC
p53 (-689bp)	CAGGACTATACAAGGCATTGGG	CGCACCACCGTGTTTAATTTCC
p53 (-426bp)	CTGTACTTGGAAGGCCTAAAGCAG	CTGTGCTCTTTCCTATCCAGCTAG
Human		
p53 (-1129bp)	GAGCTAACGGTTGAGTCTCCAAAG	CACAGGTGGGTTTCTTTAGCTCTG
p53 (-791bp)	GTTAGAAGGTTTCCCGTTCCCATC	TAGAAGCGTTCAGACTACAACTCC
p53 (-295bp)	GAGAAGAAAGGATCCAGCTGAGAG	GAGGGCAGAATTGGTGGAAATC